

Decay of bow thruster induced near-bed flow velocities at a vertical quay wall: A field measurement

Jim W.T. Tukker¹, Michel Ruijter², Charlotte V.A. van der Vorm-Hoek³, and Bas Hofland⁴

Abstract

During berthing operations of large vessels, the bow thruster jet deflecting on the quay wall and the bed can lead to high flow velocities near the bed. This may scour the bed when it is left unprotected, causing instability of the adjacent quay wall. Due to the complex flow field of the reflected jet, the decay in near-bed flow velocities perpendicular to the quay wall is unknown. This results in uncertainties in the design of bed protections, especially in the required width. In this research, the decay of the near-bed flow velocity perpendicular and parallel to the quay wall induced by a 4-channel bow thruster is studied. Field measurements have been conducted in the North Sea Port of Gent with one of the largest Dutch inland vessels. The near-bed flow velocities have been measured at multiple distances from the quay wall. For the flow velocity measurements four main parameters have been varied: the applied bow thruster power, quay wall clearance, number of thrusters, and the lateral distance between jet axis and measurement sensors. Near-bed flow velocities were measured at 26 cm from the smooth (asphalt) bed. At 1.5 and 3 m from the quay wall, the highest mean horizontal near bed flow velocities were measured in the order of 1 m/s, rapidly declining towards 0.4 m/s at 7–8.5 m from the quay wall. Maximum flow velocities reach up to 3.6 times the mean flow velocity while the measured (local) relative turbulence intensities were in the range 0.3–0.6. Comparison of the measurement results to the Dutch and German guidelines generally leads to the conclusion that these guidelines are conservative. In addition, the dependency of the velocity on the total travelled distance by the jet as given in the Dutch method is not reflected in the measurement results. Furthermore, fundamentally different outcomes on the influence of the quay wall clearance on the near-bed flow velocity have been found. Further studies with different vessels and direct measurement of the efflux velocity of the thrusters are recommended.

Keywords

Bow thruster, Propeller jet, Bed protection, Quay wall, Turbulence

¹jimtukker@gmail.com, Delft University of Technology, Delft, The Netherlands

²michel.ruijter@rws.nl Rijkswaterstaat, The Netherlands

³charlotte.vander.vorm@rws.nl, Rijkswaterstaat, The Netherlands

⁴B.Hofland@tudelft.nl, Delft University of Technology, Delft, The Netherlands


Research Article. **Submitted:** 26 April 2024. **Reviewed:** 16 December 2024. **Accepted** after double-anonymous review: 16 December 2024. **Published:** 30 December 2024.

DOI: 10.59490/jchs.2024.0040

Cite as: Tukker, J., Ruijter, M., Van der Vorm-Hoek, C., & Hofland, B. Decay of bow thruster induced near-bed flow velocities at a vertical quay wall: A field measurement. *Journal of Coastal and Hydraulic Structures*. Retrieved from <https://journals.open.tudelft.nl/jchs/article/view/7525>

This paper is part of the **Thematic Series** of selected papers on advances in physical modelling and measurement of Coastal Engineering issues, as presented on the Coastlab Conference in Delft in 2024.



The Journal of Coastal and Hydraulic Structures is a community-based, free, and open access journal for the dissemination of high-quality knowledge on the engineering science of coastal and hydraulic structures. This paper has been written and reviewed with care. However, the authors and the journal do not accept any liability which might arise from use of its contents. Copyright ©2023 by the authors. This journal paper is published under a CC-BY-4.0 license, which allows anyone to redistribute, mix and adapt, as long as credit is given to the authors. 

1 Introduction

During berthing operations vessels use bow thrusters to improve their manoeuvrability, reducing their reliance on tugboats. While manoeuvring, the transversal bow thruster jet reflects on the quay wall and is partially directed towards the bed. At the intersection between the quay wall and the bed, the jet reflects again, leading to a bottom jet perpendicular to the quay wall (Figure 1). The interaction of the jet with the ship's hull, the quay wall and bed generates a complex and turbulent flow pattern with high velocities near the bed (Cantoni et al., 2023). This results in significant hydraulic forces on the bed, and if left unprotected, scour may develop, potentially leading to instability of the quay wall (Roubos et al., 2014). Therefore, a thorough understanding of these complex and turbulent flow patterns of the jet within its confined environment is essential to accurately quantify potential scour damage and designing effective protective measures (Hamill & Kee, 2016). Furthermore, the shipping industry has seen continuous development, primarily characterized by the increasing size of inland- and sea-going vessels (Looye, 2021; OECD, 2015; Weenen et al., 2020). As vessels have grown in size, with deeper draughts, more power and larger thruster diameters, the hydraulic loads on quay walls and bed protections of berthing facilities have increased (Roubos & Verhagen, 2007).

The fundamental characteristics of jets include diffusion, the formation of mixing layers, and the additional turbulence resulting from the reduction in flow velocities (Hoffmans & Verheij, 2011). Knowledge on the flow field of propeller jets is founded upon the similarities to a plain water jet as studied by Albertson et al. (1950) by means of the axial momentum theory. Building on Albertson et al. (1950), various physical model studies, including those by Fuehrer and Römisch (1977), Blaauw & Van de Kaa (1978), Berger et al. (1981) and Verheij (1983), have developed semi-empirical relations to describe the velocity field within propeller jets. Additionally, a comprehensive review of the equations used to predict velocity distributions in propeller jets is provided by Lam et al. (2011).

Although substantial research has been conducted on the flow field of an unconfined propeller jet, there has been less focus on propeller jets near confining boundaries, such as the (sea)bed and quay walls, which are commonly encountered in navigational channels and port basins (Wei & Chiew, 2019). Studies on the flow field and hydraulic loads of confined propeller jets include Blokland (1996), Schmidt (1998), Johnston et al. (2013), Wei et al. (2017), Abramowicz-Gerigk et al. (2018) and Cantoni et al. (2023). Current empirical methods for determining the flow velocities within a propeller jet reflected on a vertical quay wall are based on limited vessel configurations and (bow) thruster types (Blokland, 1996; Schmidt, 1998). These methods rely on the simplistic 'folding' of the jet around the quay wall and the bed. The Dutch method to determine the near-bed flow velocities induced by the reflected jet are based on field measurements by Blokland (1996) with the main thruster of a tugboat in the Port of Rotterdam. Whereas the German method is based on scale model tests by Schmidt (1998) using the bow thruster of a sea-going vessel. Schmidt (1998) described the simplified two-dimensional flow pattern of a reflected jet on a vertical quay wall by identifying five different flow zones (Figure 1). A sixth flow zone, the inflow zone, has been identified by Cantoni et al. (2023) specifically for channel type bow thrusters. Currently, guidelines for designing bed protections, where the aforementioned methods are more extensively elaborated, include BAW (2010), PIANC (2015) and the Rock Manual (CIRIA et al., 2007).

Discrepancies in near-bed flow velocities have been found between theoretical values from current design guidelines and those obtained from field measurements, scale models and numerical models of confined propeller jets. A CFD study, validated by field measurements, by DHI (2016) for the Port of Hamburg measuring near-bed flow velocities at an embankment resulted in flow velocities being approximately 30% lower than those predicted by the BAW (2010) design guidelines. Similarly, scale model tests by Deltares (2015), measuring the near-bed flow velocities of a reflected bow thruster jet at a vertical quay wall, found that the Dutch method (Blokland, 1996) was generally conservative, with measured near-bed flow velocity values averaging 40% lower than theoretical predictions for quay wall clearances up to $5.5 D_t$. The study also found asymmetrical flow patterns and varying distances from the quay wall where the maximum flow velocity was measured. Additionally, the extend of the reflected bottom jet perpendicular to the quay wall varied during the measurement. The latter questions the current design guidelines for bed protection widths, which is based on vessel characteristics rather than the extent of the reflected bottom jet (PIANC, 2015). Consistent with these findings, field measurements by Cantoni et al. (2023) in the Port of Rotterdam, using an inland vessel with a 4-channel bow thruster, showed that both the Dutch and German methods overestimate near-bed flow velocities of a reflected jet at a vertical quay wall for small under keel clearances ($\sim 2 D_t$) and small quay wall clearances ($< 4 D_t$).

The aforementioned discrepancies highlight the need for further research on confined propeller jets, particularly the reflected bow thruster jet on a vertical quay wall with small under keel and quay wall clearances. This situation is very common for inland vessels during manoeuvring in ports and waterways. Based on these discrepancies, especially found by Cantoni et al. (2023), the question arises whether the Dutch and German method can accurately predict the near-bed flow velocities after reflection on a vertical quay wall for an inland vessel using a 4-channel bow thruster. Therefore, new field measurements have been conducted, focussing on the near-bed flow velocities induced by a reflected bow thruster jet of a 4-channel bow thruster used by in inland vessel at various distances from the quay. The aim is to determine the decay in near-bed flow velocities perpendicular to the quay wall, including the extent of the bottom jet, and to evaluate the measurement results against current design guidelines. The eventual goal where this research contributes to is to optimize bottom protections and their required width, which is of significant interest to the industry for ports and waterways. This study also seeks to gain additional insights into the locations where maximum flow velocities are measured and to observe asymmetrical flow patterns.

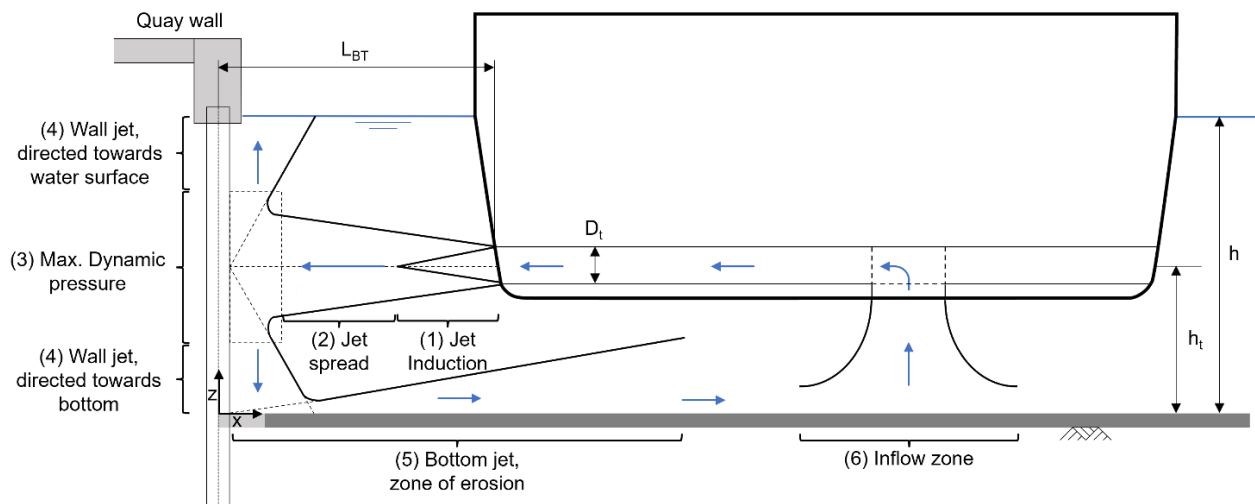


Figure 1: Cross-section of a channel type bow thruster in an inland vessel showing the five flow zones identified by Schmidt (1998) and the sixth inflow zone for channel type bow thrusters as found by Cantoni et al. (2023). Note: this is a simplified 2D representation of a complex 3D flow field.

In Section 2 the test setup, instrumentation, and post-processing methods are elaborated. In Section 3 the obtained results are presented. Next, in Section 4 the results are compared to the current guidelines. Furthermore, the possible applications of these results on current bed protection design are discussed. Followed by the discussion in Section 5 and the conclusions in Section 6.

2 Methodology

Building on the uncertainties and limitations of current guidelines in determining the flow attack on the bed, initial field measurements were conducted as a pilot in November 2018 in the Port of Rotterdam to identify effective measurement techniques and setups (Deltares, 2018). Following these preliminary measurements, Cantoni et al. (2023) performed further field studies to gain a better understanding of the flow velocities near the bed. Utilizing these findings and lessons learned, new field measurements were executed from the 28th of September to the 1st of October 2020 in the North Sea Port of Gent at the Moervaart quay wall, located at 51°08'14.19" N, 3°47'23.95" E (WGS84) (Tukker, 2021).

The measurements involved the Somtrans XXV, which falls within the CEMT VIa Rijnmax class, one of the largest classes of inland vessels in the Netherlands. The dimensions of Dutch inland waterways and ports are based on this class, leading to small under keel clearances due to its large draught (up to 4.0 m). Flow velocities near the bed, induced by the reflected bow thruster jet, were measured using Acoustic Doppler Velocimeters (ADV) and Ott current meters (Ott) placed on a scaffolding measurement frame on the bed, which will be elaborated in more detail in section 2.2.

A total of 24 different tests were conducted, varying the amount of power delivered by the bow thruster (P_t), the used bow thruster (BT) and the position of the vessel relative to the sensors and quay wall. After the field measurements, the data retrieved from the ADVs and Ott meters were post-processed before analysis.

2.1 Measurement vessel and site

An impression of the Somtrans XXV moored to quay wall at bollard 28 is given in Figure 2a while the top view of the measurement site is illustrated in Figure 2b. It has two Verhaar Omega 31130-4K 4-channel bow thrusters with each 394 kW. The bow thruster channels have a rectangular shape of 1.10 m wide by 0.82 m high, resulting in an equivalent circular bow thruster diameter (D_t) of 1.07 m, calculated as the diameter of a circle with the same cross-sectional area using the formula $\sqrt{\frac{4 \cdot a \cdot b}{\pi}}$, where a is the width and b the height of the bow thruster outlet.

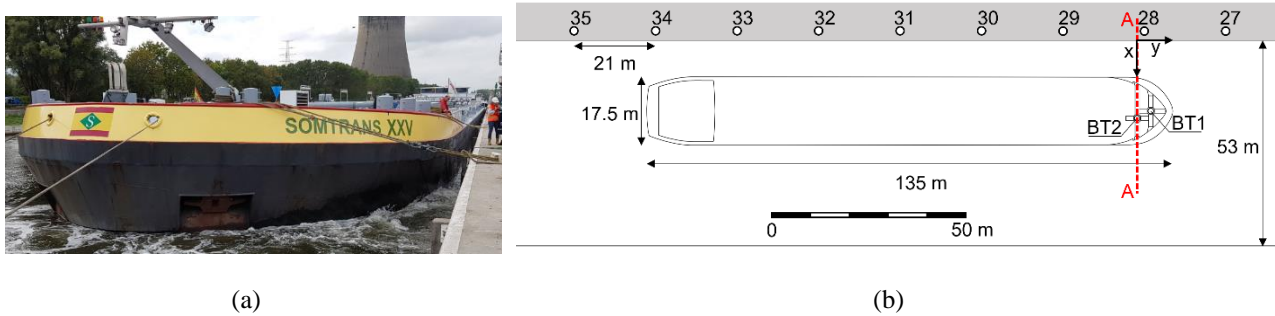


Figure 2: (a) Somtrans XXV fully loaded with Nafta during the measurements on Wednesday the 30th of September 2020. (b) The Moervaart quay wall from bollard 27 to bollard 35 including the dimensions of the Somtrans XXV.

The quay wall consists out of a sheet pile wall with a concrete cap at the top having a height of 1.8 m. The bed protection has a total width of 25 m composed out of 1 m colloidal concrete at the sheet pile wall followed by 20 m of asphalt mattresses and 4 m rip-rap. In addition, there is a small layer of sludge on top of the bed protection of approximately 0.05-0.10 m observed by the diving team. In Figure 3a cross-section of the quay wall and vessel at bow thruster 2 and the corresponding bed protection is illustrated with the main dimensions of the measurement site. During the measurement campaign the water depth was measured by pressure sensors recording a fluctuation in the water level in the range of ± 0.04 m around the measured depth of 6.4 m (Tukker, 2021).

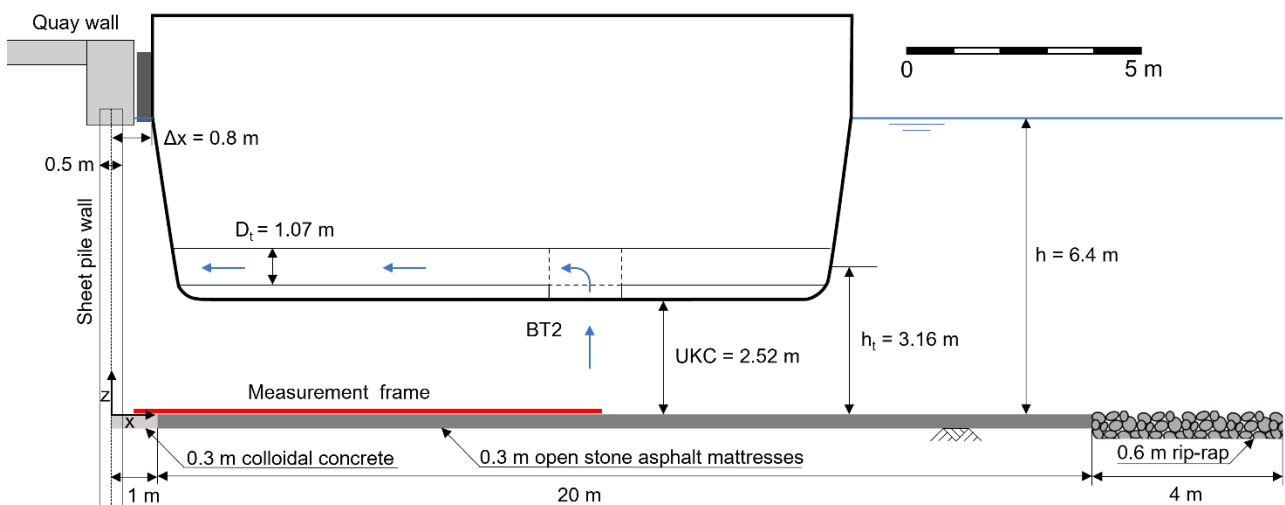


Figure 3: Two-dimensional cross section of the quay wall and vessel at location A-A (Figure 2b) at bow thruster 2 (BT2) including the bed protection and the location of the measurement frame in red.

The vessel was securely moored at both the bow and stern using multiple lines angled strategically to maintain its position (Figure 2a). During the measurements, the thruster effect pushed the vessel away from the quay wall, increasing tension on the mooring lines keeping the vessel in position. Once the bow thruster reached the required power, the jet was developed and the flow velocities stabilized, the x - and y -position of the vessel was measured. Although continuous measurements of x and y were not conducted throughout the test duration, the accuracy in both directions is estimated to be within 10 cm due to the vessel being tightly moored during the tests. Detailed metadata of the vessel's position for each test is provided in Annex A.

2.2 Measurement set-up

The near-bed flow velocities were measured with four Nortek Vector ADVs (Nortek, 2018) and two Ott C31 current meters (OTT-HydroMet, 2021) mounted on a measurement frame. The coordinates and setup of the sensors are detailed in Table 1. Each sensor sampled continuously throughout the measurement tests. Salinity was set to 0 ppt to reflect the freshwater conditions of the measurement site. The Nortek Vector ADV were operated using Nortek's Vector software version 1.39.09. The OTT C31 were programmed by one of the authors based on the calibration sheets of the OTT meters to determine the flow velocity based on the measured number of revolutions.

The measurement frame consists out of 0.05 m diameter standard scaffolding of 9.92 m long and 1.35 m wide with quay-parallel beams of 0.28 m increments. It was placed flat on the bed with 0.8 m between the sheet pile wall centreline and the first parallel beam. The centreline of the frame was vertically aligned with the stairs located close to bollard 28 as the visual reference point defining $y = 0$ (Figure 5Fout! Verwijzingsbron niet gevonden.). The positive y -direction is parallel to the quay wall in the direction of bollard 27 (Figure 2b). The positive x -direction is perpendicular to the quay wall towards the open channel with the centreline of the sheet pile wall defined as $x=0$ (Figure 5Fout! Verwijzingsbron niet gevonden.). The positive z -direction is upwards from the bed towards the water surface with the bed defined as $z=0$ (Figure 3).

The ADV's had a spatial resolution in x -direction of ~ 1.5 m close to quay wall (ADV1 and ADV2) and ~ 2 m further away from the quay wall (ADV3 and ADV4) as illustrated in Fout! Verwijzingsbron niet gevonden.. The first Ott meter (Ott1) measured at the same x -coordinate as ADV2 to compare the measured near-bed flow velocities of Ott1 with ADV2 and ensure redundancy in the measurement data. The second Ott meter (Ott2) was used as an extra spatial measurement point in x -direction at approximately 1 m from ADV4. Note that ADV4 is mounted horizontally on the measurement frame. Therefore, its height above the bed is lower than ADV1-3 which are mounted vertically (Tukker, 2021). The sensor coordinates from Table 1 are plotted in black in Figure 4. The starting position of the measurements is vessel position 1 when the centreline of BT2 is aligned with the sensors. The centreline of BT2 is marked on the vessel as the reference point for the measurements. In addition, a measurement line is attached to the side of the vessel to determine how much the vessel is moved in y -direction parallel to the quay wall.

Table 1: Coordinates of the sensors corresponding to the defined reference system and their measurement settings (Nortek, 2024; OTT-HydroMet, 2021).

Sensor	x [m]	y [m]	z [m]	Sampling frequency [Hz]	(Nominal) velocity range [m/s]	Accuracy	Coordinate system
ADV1	1.50	0	0.36	64	± 7.00	$\pm 0.5\% \pm 1$ mm/s	XYZ
ADV2	3.15	0	0.36	64	± 7.00	$\pm 0.5\% \pm 1$ mm/s	XYZ
ADV3	5.15	0.06	0.40	16	± 7.00	$\pm 0.5\% \pm 1$ mm/s	XYZ
ADV4	7.29	-0.08	0.24	8	± 7.00	$\pm 0.5\% \pm 1$ mm/s	XYZ
Ott1	3.15	0.53	0.24	1 pulse/revolution	0.025-10	$\pm 2\%$	-
Ott2	8.45	0.43	0.24	1 pulse/revolution	0.025-10	$\pm 2\%$	-

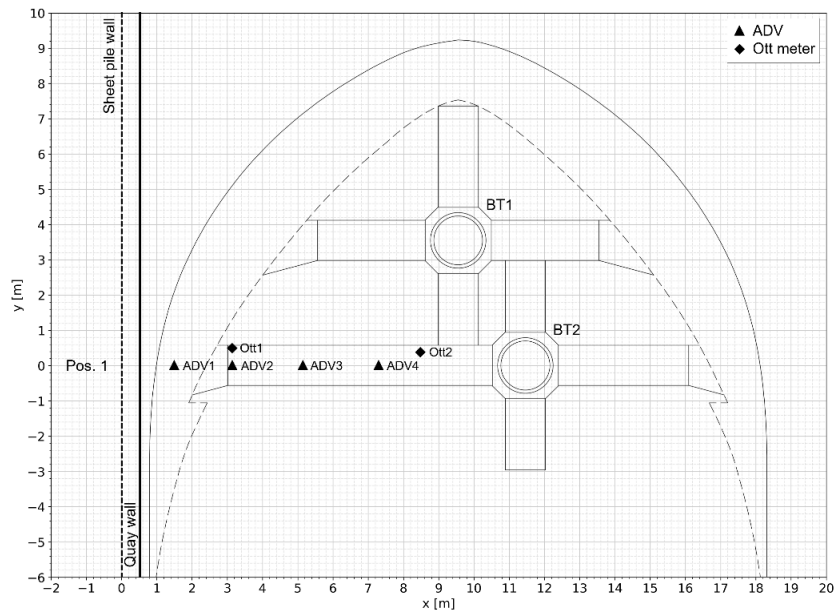


Figure 4: Overview of sensors coordinates with respect to the reference system. The dashed contours of the vessel indicate the keel while the solid lines indicate the top of the hull. The black markers correspond to the sensor coordinates as listed in Table 1 with the vessel in position 1.

2.2.1 Measurement parameters

During the measurements, four parameters were changed for every test: the applied power (P_i) of the bow thruster (1), the used bow thruster (BT1, BT2 or BT1&2) (2), the distance in y-direction between the axis of the used bow thruster channel and the sensors (Δy) (3) and the distance between quay and vessel (Δx) (4). The measurement parameters including the schematized measurement set-up are illustrated in Figure 5.

- (1) At the bridge of the vessel the power percentage of the bow thruster was altered between 25%, 50% and 90% while the corresponding RPM was read off from the display (Table 2). The 90% power step was the maximum power percentage that could be set corresponding to the maximum RPM of the bow thruster of 1800. Therefore, it is assumed that at 90% power percentage the maximum power P_i of 394 kW was applied.
- (2) The second parameter that was altered is the used bow thruster. Either bow thruster 1 (BT1), bow thruster 2 (BT2) or both simultaneously were activated resulting in three different bow thruster configurations. Due to the different position of the bow thrusters in the bow they have different channel lengths and quay wall clearances L_{BT1} and L_{BT2} (Figure 5).
- (3) The third parameter is the along-quay distance Δy . This is defined as the difference in y-coordinates between the considered bow thruster axis and the sensors. The vessel was moved to a total of six different positions parallel to the quay wall. However, not every bow thruster was tested for each position (Table 3) resulting in four different values for Δy being analysed. For BT1 $\Delta y = 2$ m, 0 m, -1.5 m and -3.5 m (Figure 14) while for BT2 $\Delta y = 3.5$ m, 2 m, 0 m and -2 m (Figure 15). For BT1&2 the axis of the bow thruster is defined in the middle between BT1 and BT2 for which the vessel was moved to $\Delta y = 1.75$ m, 0 m, -1.75 m and -3.75 m (Figure 16).
- (4) The fourth parameter is the vessel clearance which is the distance in between the vessel and the sheet-pile wall (Δx). The most applied quay wall clearance was $\Delta x = 0.8$ m, when the vessel was moored to the quay. Afterwards, Δx is increased to 3 m and 5 m corresponding to vessel position 7 and 8 in Table 3. As the bow thruster outlet of BT1 and BT2 are not at the same position in the hull, a total of six different quay wall clearances (L_{BT}) are obtained.

Table 2: RPM of the bow thruster with corresponding power load in % and P_t .

Power load [%]	RPM	P_t [kW]
25	940	98.5
50	1440	197
90	1800	394

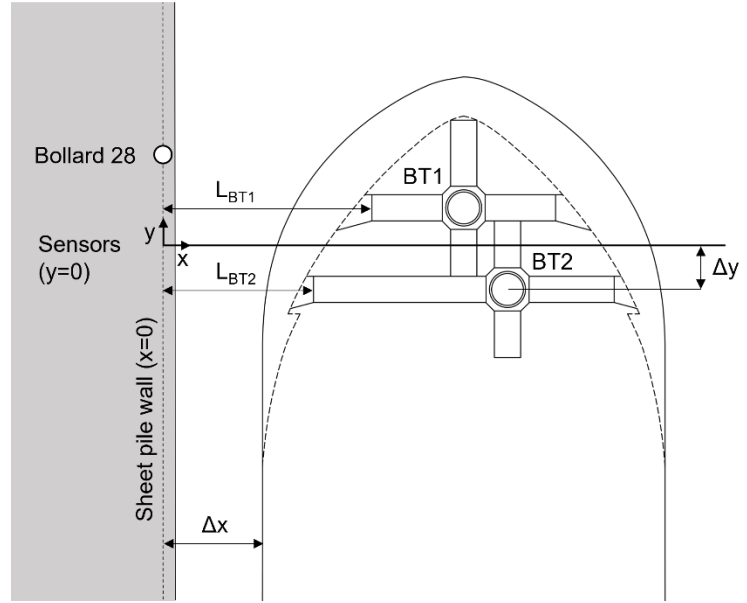


Figure 5: Top view of the outlines of the vessel at the quay wall with the varied measurement parameters. Where L_{BT1} and L_{BT2} are the quay wall clearance of BT1 and BT2, Δx the vessel-quay clearance and Δy the difference in y-coordinate between the axis of the considered bow thruster and the sensors.

2.2.2 Vessel positions

By moving the vessel in y-direction along the quay wall (Δy) and increasing the distance between the vessel and the sheet-pile wall (Δx), a total of eight different vessel positions were established during the measurements. For vessel positions 1-6 the vessel was only moved in the y-direction along the quay wall to create extra spatial measurement points. During these vessel positions the vessel was moored directly against the quay wall with $\Delta x = 0.8$ m (Figure 2a). For vessel position 1-3, the vessel was positioned such that the axis of BT2 was directly above the sensors ($\Delta y = 0$ m), 2 m below the sensors ($\Delta y = 2$ m) and 2 m above the sensors ($\Delta y = -2$ m), as illustrated in Figure 6. For vessel positions 4-6, the vessel was similarly positioned so that the axis of BT1 was directly above the sensors ($\Delta y = 0$ m), 2 m below the sensors ($\Delta y = 2$ m) and 1.75 m above the sensors ($\Delta y = -1.75$ m), as illustrated in Figure 7. When BT1 was at $\Delta y = -1.75$ m the sensors were located midway between the axis of BT1 and BT2. Continuing from vessel position 6, the vessel was moved away from the quay wall to $\Delta x = 3$ m and 5 m for vessel position 7 and 8, respectively, while maintaining the y-position ($\Delta y = -1.75$ m) with respect to BT1 to study the influence of the quay wall clearance on the measured near bed flow velocities.

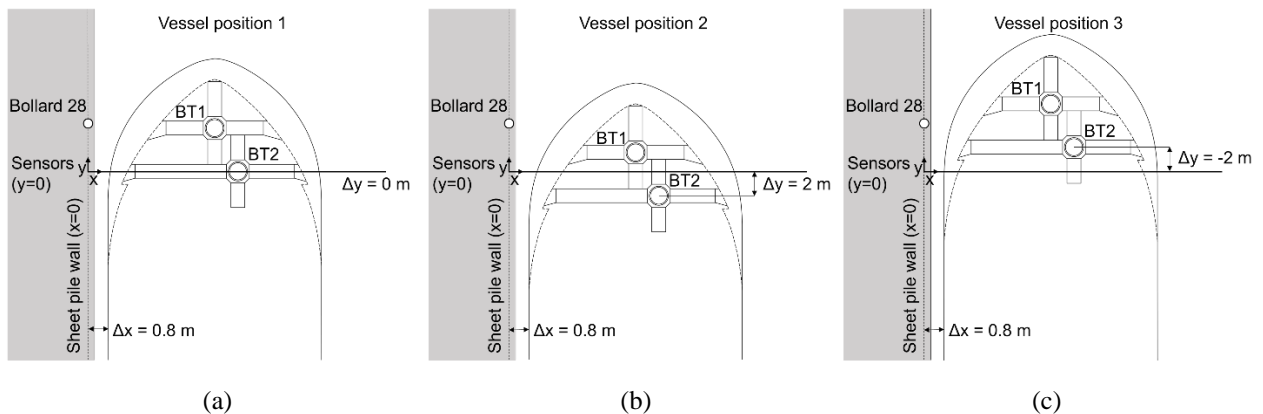


Figure 6: Vessel positions 1-3 where $\Delta y = 0$ m (a), $\Delta y = 2$ m (b) and $\Delta y = -2$ m (c) with respect to the axis of BT2.

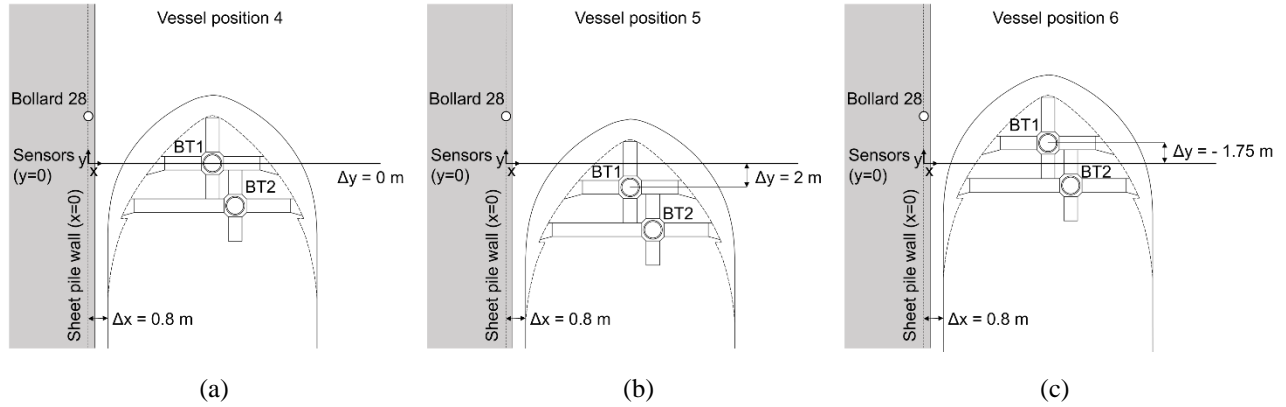


Figure 7: Vessel positions 4-6 where $\Delta y = 0$ m (a), $\Delta y = 2$ m (b) and $\Delta y = -1.75$ m (c) with respect to the axis of BT1.

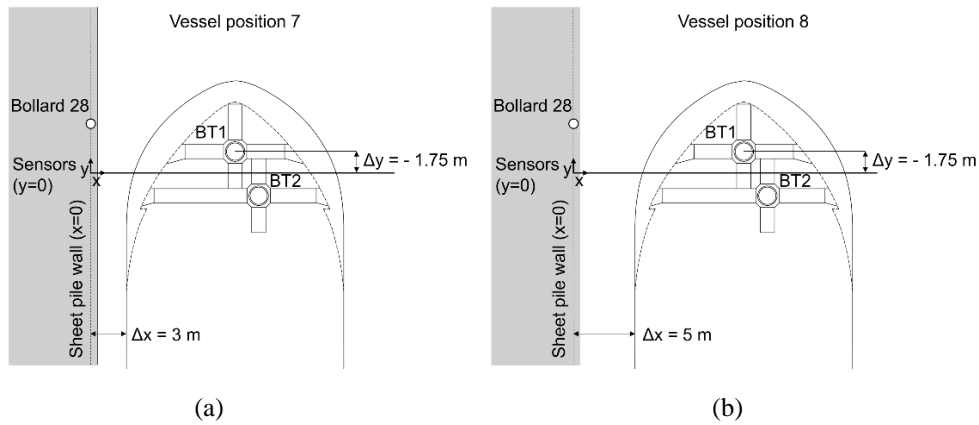


Figure 8: Vessel positions 7 and 8 where $\Delta x = 3$ m (a) and $\Delta x = 5$ m (b) while $\Delta y = -1.75$ m with respect to the axis of BT1.

2.2.3 Manoeuvring measurements

Besides the tests where the vessel was moored to the quay wall (Test 1-21 in Table 3), berthing and sailing manoeuvres were simulated during Test 22-24. First a berthing manoeuvre was executed by using the bow thrusters to move the bow away from the quay wall to a maximum Δx of approximately 15 m (Figure 9a), which took about 1.5 minutes. Afterwards, the bow thruster channel directed towards the stern of the vessel was used as forward propulsion to slowly sail over the measurement frame parallel to the quay wall with Δx of approximately 4 m (Figure 9b), which took about 2.5 minutes. The stern directed channel of the bow thrusters is directed towards the bed under a small angle, therefore the bow thruster jet directly impacts the bed resulting in a different flow situation then when the bow thruster jet reflects on the quay wall.

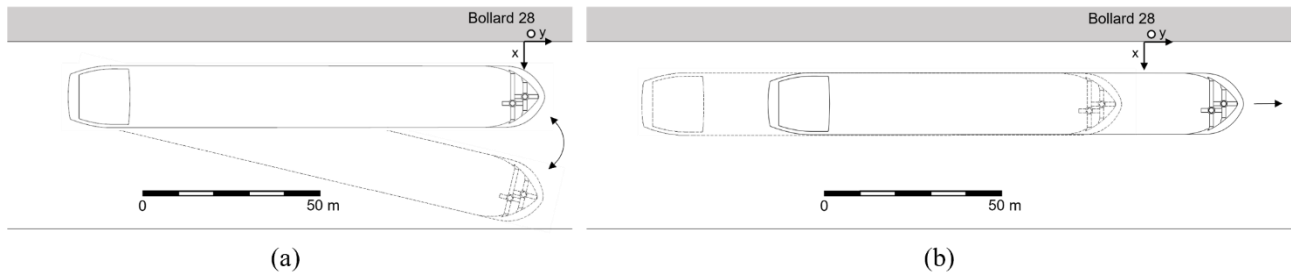


Figure 9:(a) Berthing manoeuvre of the vessel with the stern fixed to the quay wall. (b) The vessel sailing over the measurement frame with only the bow thrusters as forward propulsion.

2.2.4 Test overview

Table 3 presents an overview of the moored (Test 1-21) and manoeuvring tests (Test 22-24). Each test is divided into subtests during which the different power steps are applied for a duration of 2 min per power step.

The duration of 2 min per subtest is based on the characteristic time scale of the turbulent motion. As this is difficult to determine, engineering choices were made based on the maximum length scale of turbulent fluctuations at the bottom and the advective velocity of the turbulent motion. The maximum length scale is the distance between the thruster and the bed, while the advective velocity is the maximum flow velocity at the bed (\bar{V}_{hor}) (Deltares, 2015). Using the Dutch method (equation (8) and (9)), a maximum near-bed flow velocity of 2.65 m/s was calculated. With the bow thruster height above the bed of $h_t = 3.24$ m, the characteristic time scale T_c was 1.22 seconds. Consequently, a subtest duration of 100 times T_c , or 122 seconds (approximately 2 minutes), was chosen due to time restrictions for the measurement program, similar to the 2 minutes used per power step in the measurements by Cantoni et al. (2023).

$$T_c = \frac{h_t}{\bar{V}_{hor}} \quad (1)$$

Not every power step is measured for each test due to the instability at 50% power for BT2. Additionally, time constraints led to a focus on the 50% and 90% power steps, as these are assumed to produce the highest hydraulic loads on the bed. Several tests are excluded from further analysis: Test 1, a long measurement of 10 min to determine the minimum duration for a stable flow velocity; Test 5, which is identical to Test 8 but with slightly lower measured velocities; Tests 6 and 7, which focused on load cell measurements not considered in this study; and Test 10, which was aborted after the 50% power step.

Table 3: Test overview for the moored and the manoeuvring tests. L_{BT} is the quay wall clearance of the used bow thruster (for BT1&2 $L_{BT1\&2}$ is the average of L_{BT1} and L_{BT2}), Δx the vessel-quay clearance, deviation Δx measured at BT2 is the difference between target value and actual measured x-coordinate of BT2 during the tests, the y-coordinate of the vessel within the reference frame measured at the location of BT2 and Δy the difference in y-coordinate between the used bow thruster axis and sensors (for BT1&2 the axis is defined in between the axis of BT1 and BT2).

Test	Bow thruster (BT)	L_{BT} [m]	Vessel position	Target value Δx [m]	Deviation to Δx measured at BT2 [m]	y-coordinate vessel at BT2 [m]	Δy [m]	Power step [%]
1	2	3.09	1	0.8	0.65	0	0	25,50
2	2	3.09	1	0.8	0.53	0	0	25,50,90
3	1	5.61	1	0.8	0.04	0	-3.5	25,50,90
4	1&2	4.35	1	0.8	0.43	0	-1.75	25,50,90
5	2	3.09	2	0.8	0.40	-2	2	25,90
8	2	3.09	2	0.8	0.73	-2	2	25,90
9	1	5.61	2	0.8	0.73	-2	-1.5	25,50,90
10	1&2	4.35	2	0.8	0.79	-2	0.25	25,50
11	1	5.61	5	0.8	0.03	-5.5	2	25,50,90
12	1	5.61	4	0.8	0	-3.5	0	25,50,90
13	2	3.09	4	0.8	0	-3.5	3.5	25,90
14	1&2	4.35	4	0.8	0	-3.5	1.75	25,50,90
15	2	3.09	3	0.8	0.20	2	-2	90
16	1&2	4.35	3	0.8	0.04	2	-3.75	25,50,90
17	1&2	4.35	6	0.8	0.49	-1.75	0	50,90
18	1&2	6.55	7	3	0.47	-1.75	0	50,90
19	2	5.29	7	3	0.47	-1.75	1.75	50,90
20	1	7.81	7	3	0.48	-1.75	-1.75	50,90
21	1&2	8.55	8	5	0.63	-1.75	0	50,90
22	1&2	-	Berthing	0.8 to 15	-	Initial -1.75	Initial 0	25,50,90
23	1&2	-	Sailing	4	-	-	-10 to +10	90
24	1	-	Sailing	4	-	-	-10 to +10	90

2.3 Post-processing

The ADV data has been post-processed before analysing the measurement results in Section 3. This process involves six steps, detailed below. The first three steps are applied to the x , y and z components of the flow velocity individually. Subsequently, the post-processing continues with the horizontal flow velocity component which is the resultant of the x and y -components according to Equation (2). This represents the horizontal velocity that causes the drag force as used in the Izbash (1935) approach for rock stability of the bed. Consistent with Blokland (1996), this is used in the results to compare the flow velocity load from the measurement tests.

$$V_{hor} = \sqrt{V_x^2 + V_y^2} \quad (2)$$

- (1) A correction for the speed of sound in water was applied to the flow velocity components of ADV1 and ADV4, as these ADVs measured with a salinity of 35 ppt instead of the assumed 0 ppt for freshwater.
- (2) In this step, the data is filtered on signal strength and correlation based on the methods proposed by Nortek (2018). To quantify the data quality, a signal to (background) noise ratio of 15 dB is applied as threshold. Further, the correlation between two pulse echoes being measured by the ADV should be larger than a threshold, for which the recommended 70% was used.
- (3) For ADV1 and ADV2, a bimodal distribution with outliers was observed in the measurement data, attributed to aliasing of the Doppler signal (Goring & Nikora, 2002; Durgesh et al., 2014). These outliers were removed by applying a standard deviation filter omitting all measurements outside the range of $\bar{V} \pm 2\sigma$ (per velocity component). This filtering approach effectively eliminated the spurious outliers caused by the aliasing of the Doppler signal (Tukker, 2021).
- (4) This step evaluates the validity of statistical parameters derived from the normal distribution for flow velocities measured by the ADVs, ensuring that the velocity components conform to the normal distribution, while V_{hor} should exhibit a skewed normal distribution. Damage to bed protections is primarily caused by the extremes in flow velocities, which are especially evident in the highly turbulent jets produced by bow thrusters. In Section 3 the turbulence is quantified by the standard deviation (σ) of V_{hor} . Based on these statistical parameters a calculation value for the maximum flow velocity is defined corresponding to the mean flow velocity plus three times the standard deviation ($\bar{V}_{hor} + 3\sigma$). This definition for the maximum flow velocity is more reliable to use instead of the actual measured maximum flow velocity since the latter depends on the measurement duration and sampling frequency. Consequently, this statistical maximum flow velocity is widely adopted as the characteristic value for designing bed protections (PIANC, 2015; Schiereck & Verhagen, 2016) and will be further used for the remainder of this study to quantify the maximum flow velocity.
- (5) Measuring the flow velocity with an ADV set on a high sampling frequency and large velocity range can induce Doppler noise (Huang et al., 2020). Doppler noise is similar to white noise and caused by the intrinsic limit to the accuracy of the Doppler processing (Durgesh et al., 2014). In Figure 10, the Doppler noise is observed as a constant resulting energy level in the higher frequencies of the spectrum. To determine the correct statistical parameters for the flow velocity near the bed, a noise correction method is applied. First, the flow velocity is transformed to a power spectrum of the measured horizontal flow velocity by means of the Welch (1967) method. Secondly, the variance of the noise (σ_{noise}^2) is obtained by assuming the noise level is equal to the spectral density at the higher frequencies ($f = 32$ Hz). Subsequently, this variance due to this noise level is subtracted from the measured variance (σ^2) to determine the correct standard deviation ($\sigma_{corrected}$) by means of Equation (3). A visual representation of this method is illustrated in Figure 10, where in blue the resulting variance is indicated. In Figure 10a the noise level is clearly visible, however, in Figure 10b it is less noticeable. This is due to the increased variance at the 90% power step induced by the higher flow velocities. As a result, the variance induced by the noise constitutes a smaller proportion of the total variance during the 90% power step than during the 25% power step.

$$\sigma_{corrected} = \sqrt{\sigma^2 - \sigma_{noise}^2} \quad (3)$$

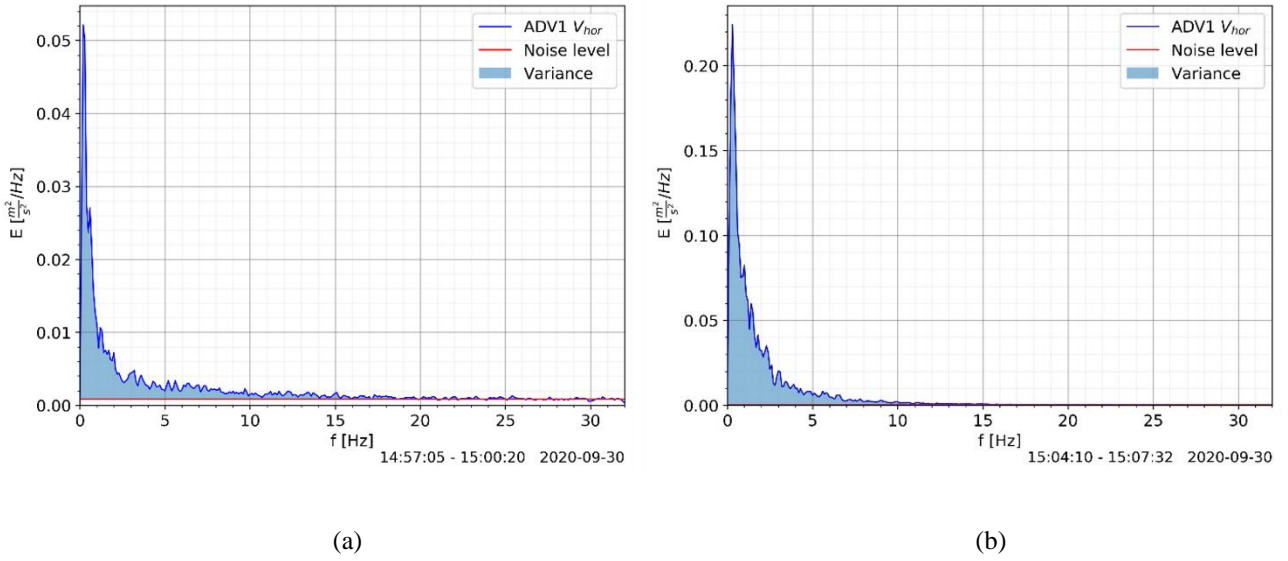


Figure 10: Noise reduction method for V_{hor} Test 4 ADV1 at 25% power (a) and 90% power (b) by means of a spectral analysis with the energy (E) on the y-axis and the frequency (Hz) on the x-axis.

3 Results

The test results for the absolute horizontal near-bed flow velocity are elaborated per measurement parameter as described in Section 2.2.1 consisting out of the applied bow thruster power (P_i), the used bow thruster, Δy and Δx . For each test the mean flow velocity (\bar{V}_{hor}) and standard deviation (σ_{hor}) are determined from which the maximum flow velocity ($V_{max} = \bar{V}_{hor} + 3\sigma_{hor}$) and relative turbulence intensity ($r_{hor} = \sigma_{hor}/\bar{V}_{hor}$) are derived. These statistical parameters are presented as function of the perpendicular distance x from the quay wall. The sensors considered in the results are ADV 1-4, represented by a circle in the figures, and Ott2, represented by a square in the figures. Positioned near ADV2, Ott1 is excluded from the result figures as it is used to compare the similarity in the statistical parameters measured by two different sensors. Both ADV2 and Ott1 measured similar values for \bar{V}_{hor} , while Ott1 measured significantly lower values for σ_{hor} , probably due to the lower dynamic response of the mechanical Ott meters. However, Ott2, located 1 m from ADV4 in positive x -direction, measured similar values for both \bar{V}_{hor} and σ_{hor} which could be due to the lower-frequency turbulence of the flow. Nevertheless, σ_{hor} measured by Ott2 should be interpreted with caution. Therefore, r_{hor} derived for Ott2 is not included in the results.

3.1 Applied power (P_i)

The effect of the applied bow thruster power is first shown for each of the statistical parameters (\bar{V}_{hor} , σ_{hor} , V_{max} and r_{hor}) per power step for all the tests where the vessel was moored to the quay wall (Test 1-21). In Figure 11, Figure 12 and Figure 13, the markers represent the average values for each sensor, while the error bars indicate the highest and lowest measured values for the corresponding statistical or derived parameters in Tests 1-21. Figure 11a shows \bar{V}_{hor} and Figure 11b shows σ_{hor} . For both parameters and all power steps a clear decay profile is observed while moving away from the quay wall (positive x). The highest values for \bar{V}_{hor} and σ_{hor} are measured close to the quay wall by ADV1 and ADV2. However, for \bar{V}_{hor} during all power steps slightly higher values are measured by ADV2 in comparison to ADV1. A similar trend is observed for σ_{hor} at 25% power. After ADV2 a clear decay is observed towards ADV4, stabilizing, or even increasing slightly towards Ott2 (fifth sensor). Focussing on the difference in power, a significant increase is observed from 25% (green) towards 50% (blue) power for all sensors. Further increasing the power towards 90% (red) does not result in a substantial increase in average values for \bar{V}_{hor} and σ_{hor} . However, the maximum values for both \bar{V}_{hor} and σ_{hor} increase, moving from 50% to 90% power. Close to the quay wall, at 50% and 90% power, \bar{V}_{hor} is in the order of 1 m/s reaching up to maxima of 1.7 m/s. Further away from the quay, the flow rapidly declines towards a more constant level of approximately 0.3-0.4 m/s at 50% and 90% power having maxima up to 1 m/s. Focussing on σ_{hor} , average values

close to the quay wall are between 0.36–0.40 m/s during the 50% and 90% power step with maxima up to 0.56 m/s. At ADV4 and Ott2 (fifth sensor), average values of σ_{hor} are in the order of 0.14–0.16 m/s with maxima up to 0.36 m/s.

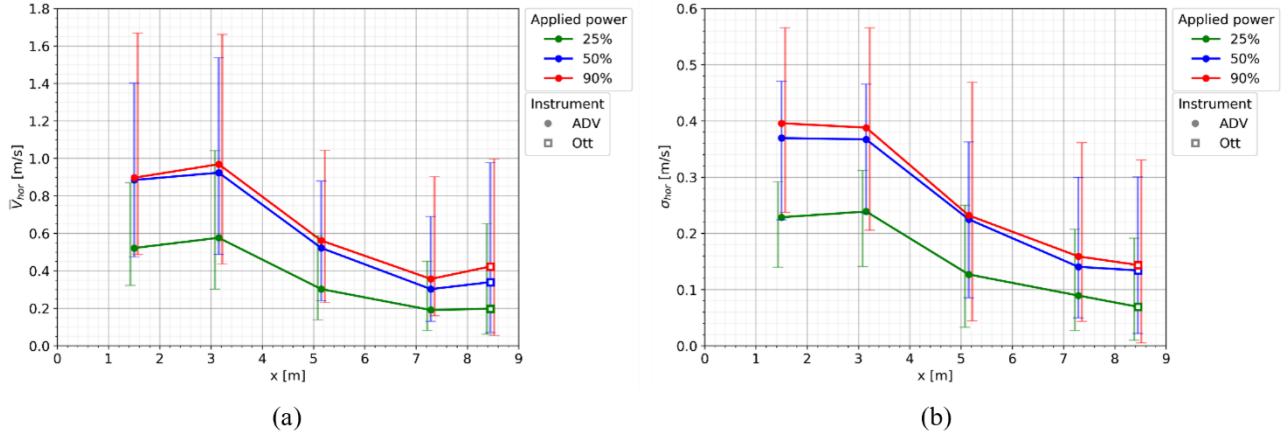


Figure 11: Average values of \bar{V}_{hor} (a) and σ_{hor} (b) for the moored tests (Test1-21) at 25%, 50% and 90% power. The markers depict the average over the tests and the error bars indicate the maximum and minimum measured value for V_{max} (a) and r_{hor} (b). The water depth was $h = 6.3$ m and the distance between the bed and the axis of BT1 and BT2 was $h_t = 3.16$ m.

For V_{max} , in Figure 12a, a similar decay trend is observed as for \bar{V}_{hor} and σ_{hor} with values ranging between 1.6–3.4 times \bar{V}_{hor} according to Equation (4). Due to the similar decay pattern observed for \bar{V}_{hor} and σ_{hor} the relative turbulence intensity ($r_{hor} = \sigma_{hor}/\bar{V}_{hor}$) does not show much variation while moving in positive x -direction from the quay wall. Generally ranging between 0.3–0.6 with an average value of 0.44 over the three power steps and ADV1-4. However, a few extremes as low as 0.2 and as high as 0.8 are also observed for the ADV3 and ADV4.

$$V_{max} = \bar{V}_{hor} + 3\sigma_{hor} \approx (1 + 3r_{hor})\bar{V}_{hor} \quad (4)$$

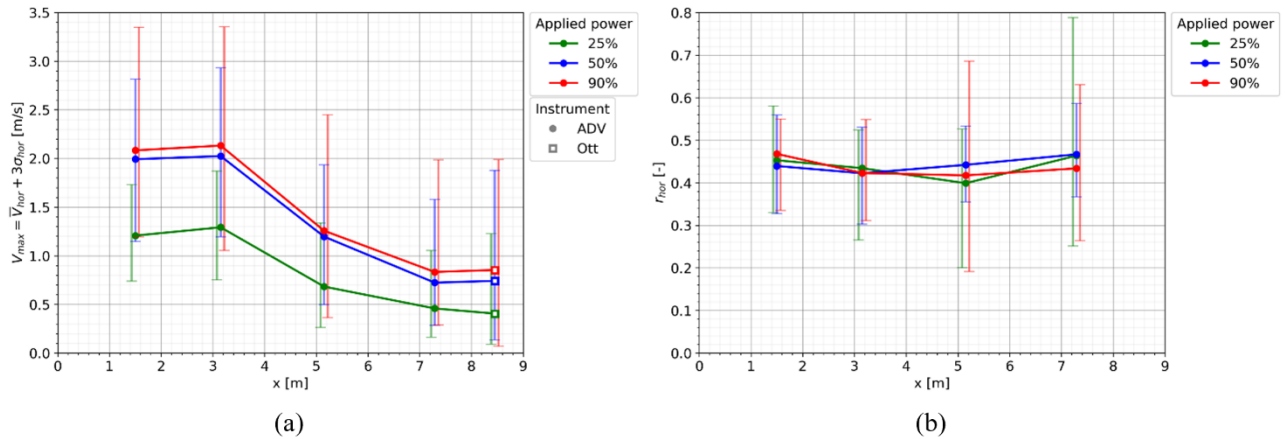


Figure 12: Average values of V_{max} (a) and r_{hor} (b) for the moored tests (Test1-21) at 25%, 50% and 90% power. The markers depict the average over the tests and the error bars indicate the maximum and minimum measured value for V_{max} (a) and r_{hor} (b). The water depth was $h = 6.3$ m and the distance between the bed and the axis of BT1 and BT2 was $h_t = 3.16$ m.

3.2 Used bow thruster

The vessel is equipped with two 4-channel bow thrusters (BT1 and BT2) where BT1 is located closer to the bow of the vessel in comparison to BT2 (Figure 5). In addition, BT1 has a shorter channel length than BT2 resulting in a different quay wall clearance. When the vessel is moored to the quay ($\Delta x = 0.8$ m) the quay wall clearances are $L_{BT1} = 5.61$ m and $L_{BT2} = 3.09$ m. In Figure 13, the average values for V_{max} are shown including the maxima and minima for the tests with

either BT1 (green), BT2 (blue) or BT1&2 (red). Three tests per BT with $\Delta x = 0.8$ m and equal or similar values for Δy are compared to each other. For BT1 these are Test 11 ($\Delta y = 2$ m), Test 12 ($\Delta y = 0$ m) and Test 9 ($\Delta y = -1.5$ m). For BT2 these are Test 8 ($\Delta y = 2$ m), Test 2 ($\Delta y = 0$ m) and Test 15 ($\Delta y = -1.5$ m). For BT1&2 these are Test 14 ($\Delta y = 1.75$ m), Test 2 ($\Delta y = 0$ m) and Test 15 ($\Delta y = -1.75$ m). For the separate bow thrusters, similar decay profiles are observed with BT1 and BT2 measuring very similar values for V_{max} . When BT1&2 are activated simultaneously significantly higher values for V_{max} are measured. The small difference in V_{max} for BT1 and BT2 can be attributed to the variation in quay wall clearance (L_{BT}), channel length and the position of the bow thruster from the sensor. Moreover, as BT1 is placed closer to the bow of the vessel, the shape of the hull at this location may significantly influence the flow compared to BT2, where the flow is more confined between the quay and the vessel. This could result in higher flow velocities parallel to the quay wall (y -direction). Further research is needed to determine which of these characteristics has the most influence on V_{max} .

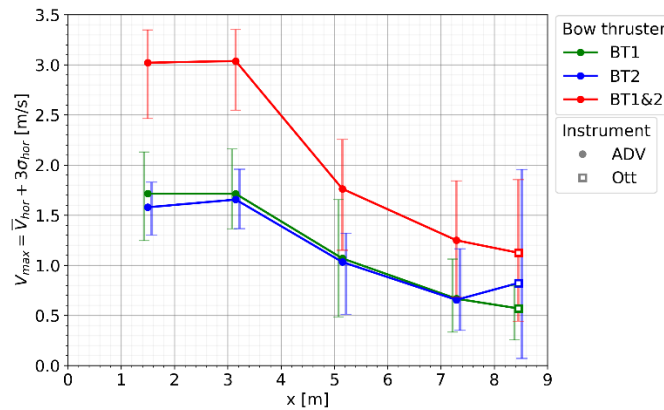


Figure 13: Average value of V_{max} for the moored tests (Test1-21) where either BT1, BT2 or BT1&2 were used. The markers depict the average over the tests and the error bars indicate the maximum and minimum measured value for V_{max} . The water depth was $h = 6.3$ m and the distance between the bed and the axis of BT1 and BT2 was $h_t = 3.16$ m.

3.3 Distance Δy between bow thruster axis and sensors

The third measurement parameter that is altered during the tests is the distance Δy between bow thruster axis and the sensors, as explained in Section 2.2.1. For BT1, BT2 and BT1&2 four different values for Δy are studied focussing on V_{max} during the 90% power step as this represents the highest hydraulic load on the bed. While Δy is varied, Δx is kept constant at $\Delta x = 0.8$ m during the considered tests in this section. In the figures labelled with (a) the top view of the vessel is illustrated with all positions of the sensors relative to the axis of the used bow thruster. In the figures labelled with (b) the corresponding test results for V_{max} during the 90% power step is illustrated.

For BT1, the top view of the vessel with considered values for Δy are given in Figure 14a while the results are illustrated in Figure 14b. Every test shows a similar decay profile as observed in Figure 13 for increasing distance x from the quay wall. The highest values for V_{max} at ADV1-4 are measured during Test 9 (green) where $\Delta y = -1.5$ m while for Ott2 (fifth sensor) slightly higher values for V_{max} were measured at $\Delta y = -3.5$ m during Test 3. From Figure 14a can be observed that the highest values for V_{max} are not measured directly underneath the bow thruster channel axis but slightly towards the stern of the vessel.

For bow thruster 2 (BT2) two exceptions to the characteristic decay profile are observed in Figure 15b. First, for $\Delta y = 0$ m (Test 2), where a strong increase in V_{max} is observed between ADV1 and ADV2. Secondly, for $\Delta y = -2$ m (Test 15) a constant V_{max} for increasing values of x is observed with a strong increase in V_{max} at $x = 8.5$ m (Ott2). Close to the quay wall, the highest values for V_{max} are measured towards the bow of the vessel and underneath the bow thruster channel whereas further from the quay wall in x -direction the highest values are measured towards the stern of the vessel (indicated by the red circles in Figure 15a).

For BT1&2 the axis of the two bow thrusters is defined as the centreline between BT1 and BT2 indicated by the solid black line in Figure 16a. Figure 16b shows the characteristic decay profiles observed in Figure 13. An exception is observed for $\Delta y = -3.75$ m (Test 16), for which a similar pattern is observed as for Test 15 of BT2, measuring relatively

constant values for V_{max} for increasing distance x from the quay wall. Close to the quay wall, the highest values for V_{max} are measured in between BT1 and BT2 at $\Delta y = 0$ m while for increasing distance x from the quay wall the highest values for V_{max} are measured towards the stern of the vessel (illustrated by the red circles in Figure 16a). This is possibly caused by the fact that the flow is vertically more confined towards the stern, as the draft is larger.

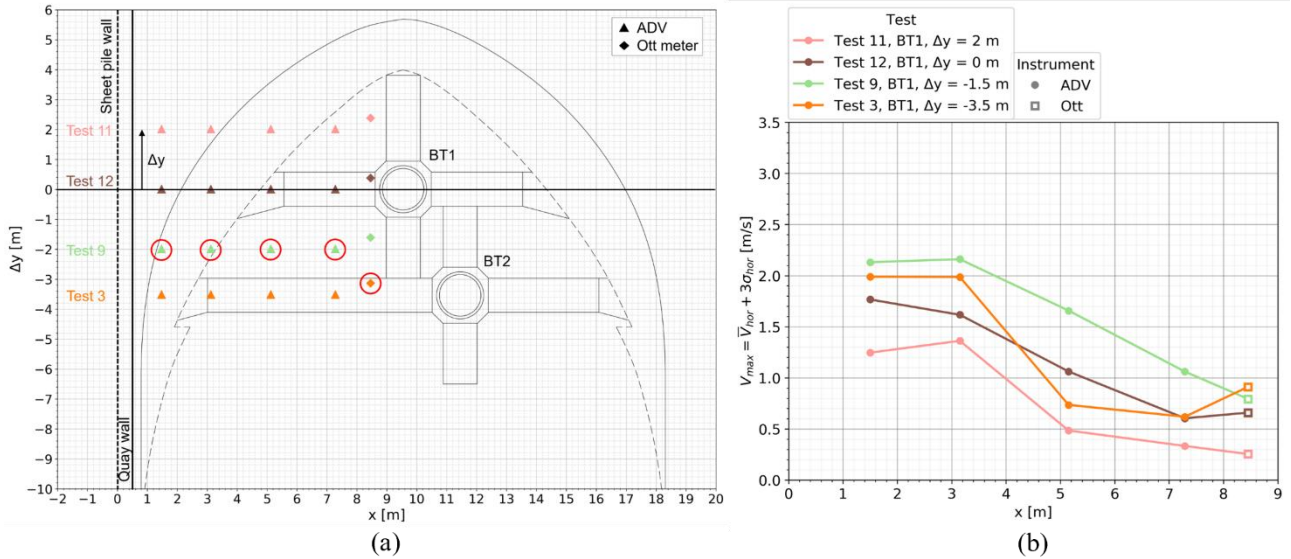


Figure 14: (a) Top view of the sensor locations for the tests when BT1 is activated, $\Delta x = 0.8$ m (Test 11,12,9 and 3) and 90% power step. The red circles indicate per sensor location (x) for which Δy the highest value for V_{max} is measured. (b) V_{max} for different Δy (-3.5, -1.5, 0 and 2 m) for these selected measurements.

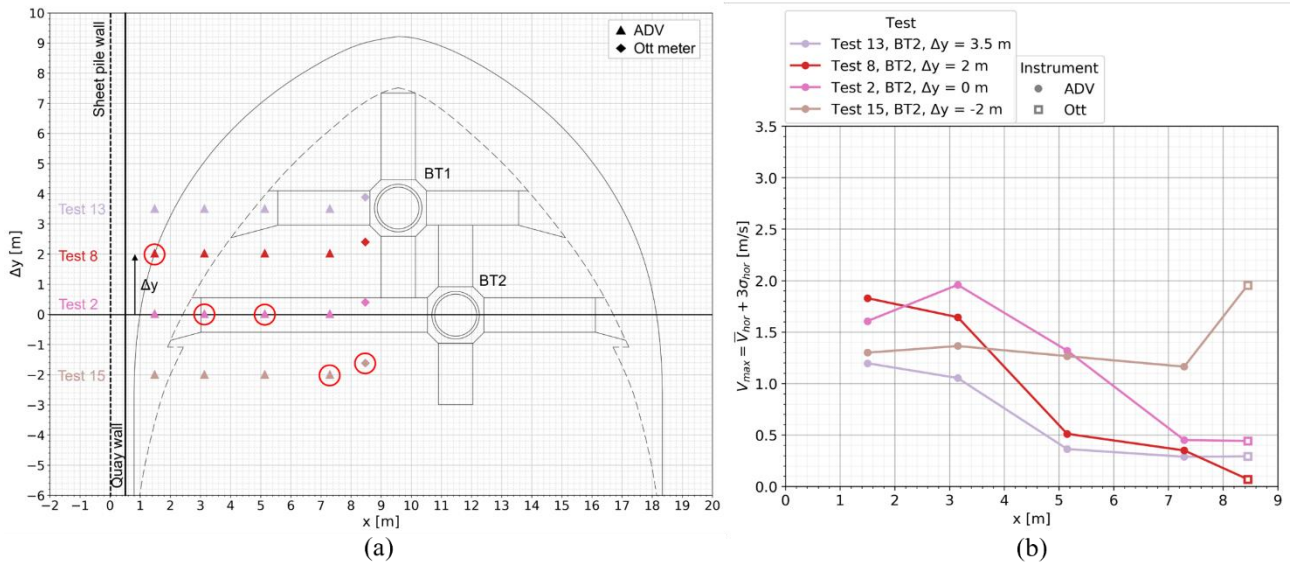


Figure 15: (a) Top view of the sensor locations for tests when BT2 is activated, Test 13, 8, 2 and 15, corresponding to $\Delta y = 3.5$ m, 2 m, 0 m and -2 m. The red circles indicate per sensor location for which Δy (or test) the highest value for V_{max} is measured. (b) Measurement results per test for V_{max} during the 90% power step.

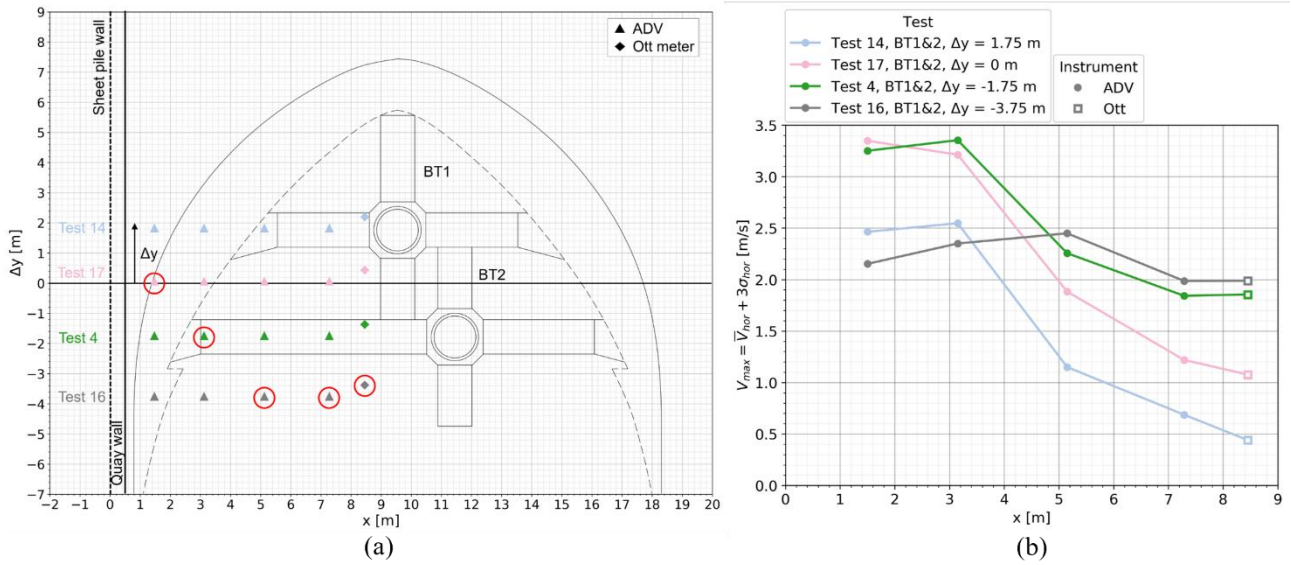


Figure 16: (a) Top view of the sensor locations for tests with BT1&2 activated simultaneously, Test 14, 17, 4 and 16, corresponding to $\Delta y = 1.75$ m, 0 m, -1.75 m and -3.75 m. The red circles indicate per sensor location for which Δy the highest value for V_{max} is measured. (b) Measurement results per test for V_{max} during the 90% power step.

3.4 Quay wall clearance (increasing Δx)

The effect of the quay wall clearance on V_{max} is investigated by comparing the profiles of V_{max} for different Δx . During these tests at 90% power all other variables are (nearly) constant. The quay-clearance Δx was varied from 0.8 m, when the vessel is moored to the quay wall (Figure 3), to 3 m and 5 m. For $\Delta x = 5$ m, measurements are conducted only for BT1&2 activated simultaneously.

In Figure 17a the results for the increase in quay wall clearance from $\Delta x = 0.8$ m to $\Delta x = 3$ m for BT1 and BT2 are illustrated. Note that for the tests with $\Delta x = 3$ m and 5 m the measurement frame was positioned with a small offset in Δy of 0.25 m, with respect to the tests with $\Delta x = 0.8$ m. For BT1, having a larger initial quay wall clearance than BT2, increasing Δx generally results in slightly (roughly 0.2 m/s) lower values for V_{max} . However, for BT2 a small increase in V_{max} of roughly 0.2 m/s is observed at every sensor for an increased clearance. This latter observation is contrary to the expectation that higher values for Δx result in lower near-bed flow velocities.

Figure 17b shows V_{max} for various quay clearances for tests with BT1&2 activated. Increasing Δx from 0.8 m to 3 m results in similar values for V_{max} . Further increasing Δx towards 5 m leads to an overall decrease in V_{max} of 0.3 to 0.5 m/s, except for the sensors furthest away from the quay wall.

3.5 Manoeuvring measurement tests

In this section the manoeuvring measurements (Test 22-24) are compared to the measurements with a moored vessel to the quay wall (Test 1-21) to analyse the difference in near-bed flow velocities between an actual berthing manoeuvre and the simplified setup (moored to the quay wall). For the manoeuvring measurements the maximum horizontal flow velocity near the bed is defined as the highest instantaneous measured flow velocity ($V_{max,inst}$) in comparison to $V_{max} = \bar{V}_{hor} + 3\sigma_{hor}$ for the moored measurements. This is due to the statistical parameters not being valid when the vessel sails over the measurement sensors. In Figure 18a, these values are given for both the berthing test (Test 22) and several moored tests with different quay wall clearances and otherwise equal variables. Lower values for $V_{max,inst}$ are measured during the berthing test at every sensor in comparison to V_{max} for the moored tests. There is one exception to this observation for ADV3, measuring slightly higher values for $V_{max,inst}$ than for V_{max} at $\Delta x = 5$ m (Test 21).

Focussing on the sailing tests (Test 23 and 24) in Figure 18b, a different profile is observed than during the other tests. When BT1&2 are activated, a horizontal line is observed with values for $V_{max,inst}$ ranging between 1.5-1.75 m/s while for BT1 a peak in $V_{max,inst}$ of 1.5 m/s is observed at ADV2. Both sailing tests show significantly lower maximum flow velocities for $x < 5$ m compared to the moored and berthing tests. For $x > 5$ m the sailing test with BT1&2 shows higher maximum flow velocities. Important to note is the difference in used channel of the used bow thruster. During the sailing tests the stern directed channel was used which is under small angle towards the bed. As $\Delta x \approx 4$ m the stern directed channel outlet of BT1 is at $x = 13.5$ m while the outlet of BT2 is at $x = 15.5$ m both falling outside the range of the sensors.

Even though the number of manoeuvring tests was limited to three tests (Test 22, 23 and 24), the manoeuvring tests did not result in high flow velocities near the bed than the moored tests.

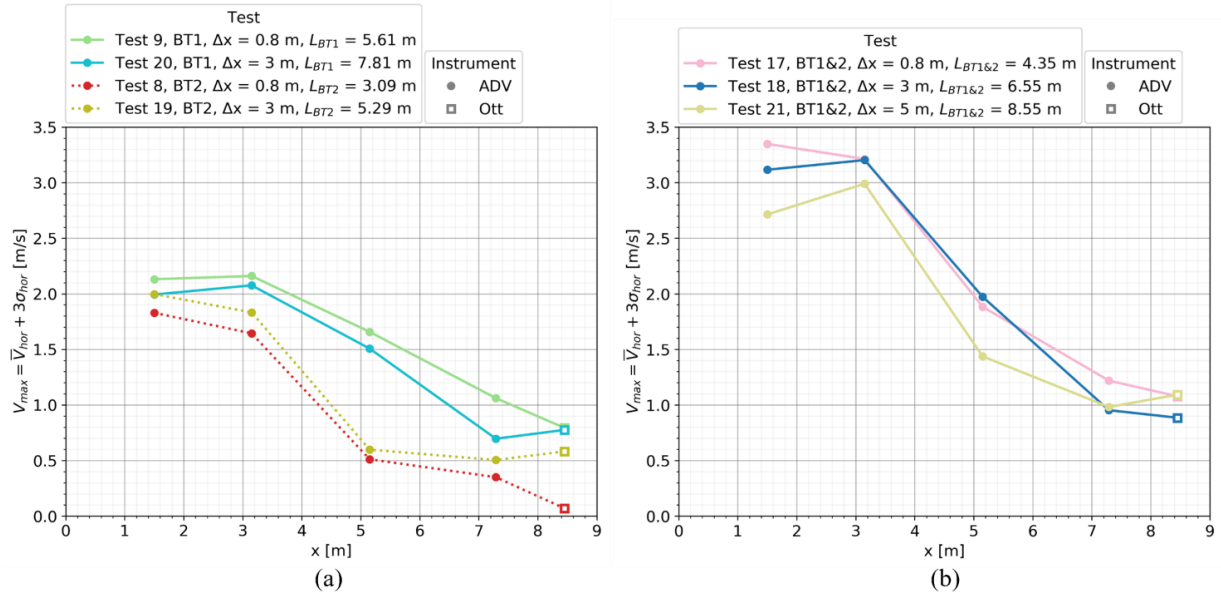


Figure 17:(a) Measurement results for BT1 and BT2 while increasing the quay wall clearance from $\Delta x = 0.8$ m to $\Delta x = 3$ m at 90% power. (b) Measurement results for BT1&2 activated simultaneously for $\Delta x = 0.8$ m, 3 m and 5 m at 90% power.

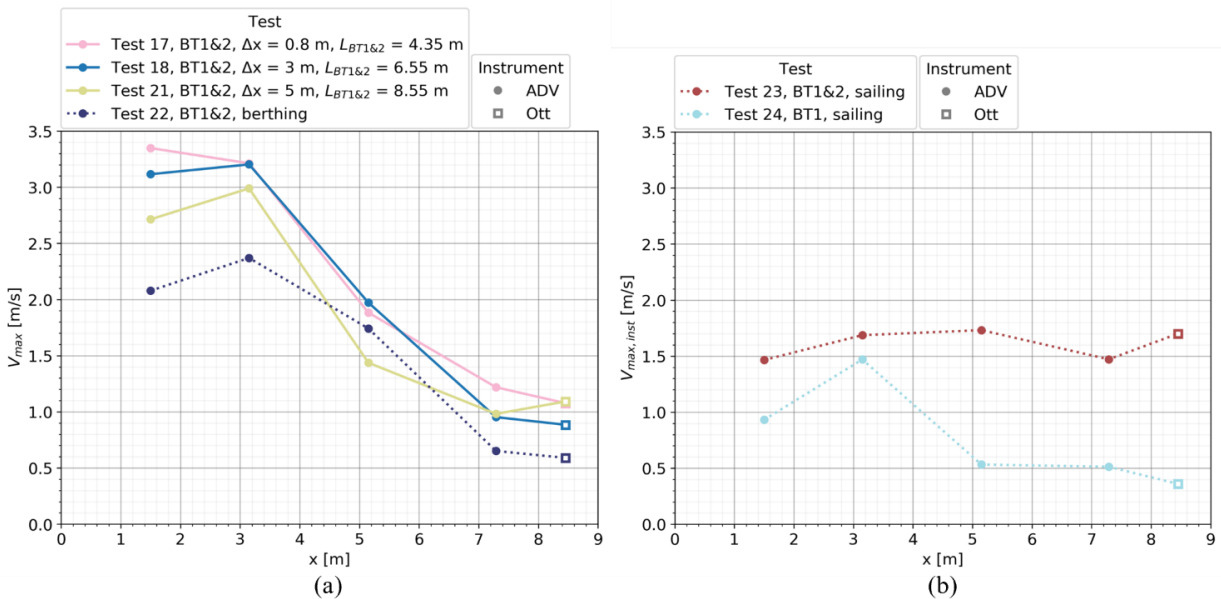


Figure 18:(a) Comparison between the moored measurement tests ($\Delta x = 0.8$ m, 3 m and 5 m) with $\Delta y = 0$ and berthing manoeuvre test ($\Delta x = 0.8 - 15$ m) when BT1&2 are activated all during 90% power. (b) Sailing manoeuvre tests for BT1 and BT1&2 at 90% power and $\Delta x = 4$ m.

4 Comparison to guidelines

The results from the field measurements were compared to theoretical predictions for the near-bed flow velocity according to empirical formulae described in commonly used guidelines such as PIANC (2015) and BAW (2010).

4.1 Maximum near-bed flow velocities

Currently used methods to determine the near-bed flow velocities induced by a bow thruster jet after reflection on a vertical quay wall are the Dutch and German method. The Dutch method is based on research by Blaauw and Van de Kaa (1978), Verheij (1983) and Blokland (1996) whereas the German method is founded on research by Fuehrer et al. (1981) and Schmidt (1998). Both methods depend on the efflux velocity V_0 calculated according to Equation (5) (Blaauw & Van de Kaa, 1978), consisting out of the bow thruster power (P_t), water density (ρ_w), thruster diameter (D_t) and energy loss factor (ξ) for bow thrusters ($\xi = 0.9$ for channel type bow thrusters of inland vessels according to Meijer & Verheij (1993)).

$$V_0 = \xi \cdot 1.17 \cdot \left(\frac{P_t}{\rho_w \cdot D_t^2} \right)^{1/3} \quad (5)$$

During berthing manoeuvres, the bow thruster jet deflects on the quay wall at location (1) after which part of the jet deflects downwards towards the bed where it deflects again at location (2) in the corner between the quay and the bed. According to this calculation model, after deflection on the bed, the highest (virtual) near-bed flow velocities are expected. The deflected bow thruster jet spreads over the bed in positive x-direction from the quay wall while the near-bed flow velocity decays for increasing distance x (location (3)). The described locations are illustrated in Figure 19.

An upper limit for the mean flow velocity in x-direction at the bed (location 2) can be calculated according to the German method described by Equation (6) and (7). The German method is primarily based on the scale model measurements by Schmidt (1998) who measured the mean near-bed flow velocity in x-direction (\bar{V}_x). In Equation (6) and (7) a_L is a dimensionless coefficient based on the bow thruster diameter D_t and the distance L_{BT} between the bow thruster outlet and the quay wall.

$$\bar{V}_{x,German} = a_L \cdot V_0 \cdot \left(\frac{h_t}{D_t} \right)^{-1.15} \quad \text{for } \frac{L_{BT}}{D_t} < 1.9 \quad \text{with } a_L = 10.6 \cdot \left(\frac{L_{BT}}{D_t} \right)^{-1.0} \quad (6)$$

$$\bar{V}_{x,German} = a_L \cdot 1.9 \cdot V_0 \cdot \left(\frac{L_{BT}}{D_t} \right)^{-1.0} \left(\frac{h_t}{D_t} \right)^{-1.15} \quad \text{for } \frac{L_{BT}}{D_t} > 1.9 \quad (7)$$

The Dutch method is mainly founded on the full-scale measurements by Blokland (1996) who based the Dutch method on the upper limit of the measured mean horizontal near-bed flow velocity (\bar{V}_{hor}), as applied in this paper. The Dutch method calculates the near-bed flow velocity according to Equation (8) and Equation (9) just after deflection of the jet on the bed at location (2) when $x = 0$ and location (3) when $x > 0$. Therefore, the Dutch method gives a relation for the decay in near-bed flow velocity based on the total travelled distance of the jet composed out of the sum of L_{BT} , h_t and x (Figure 19).

$$\bar{V}_{hor,Dutch} = 1.0 \cdot V_0 \cdot \frac{D_t}{h_t} \quad \text{for } 1.0 < \frac{(L_{BT} + x)}{h_t} < 1.8 \quad (8)$$

$$\bar{V}_{hor,Dutch} = 2.8 \cdot V_0 \cdot \frac{D_t}{L_{BT} + h_t + x} \quad \text{for } \frac{(L_{BT} + x)}{h_t} > 1.8 \quad (9)$$

An alternative to the Dutch method to determine the decay in \bar{V}_{hor} at location (3) for increasing values of x from the quay wall is Equation (10) as mentioned in the BAW (2010). Where $\bar{V}_{hor,Dutch(x=0)}$ is the near-bed flow velocity just after deflection at location (2) for $x = 0$ calculated according to either Equation (8) or Equation (9). However, as the source for this method is unknown the use of $\bar{V}_{hor,Dutch(x=0)}$ is questionable.

$$\bar{V}_{hor,Dutch-BAW} = \bar{V}_{hor,Dutch(x=0)} \cdot \left(\frac{L_{BT} + h_t}{L_{BT} + h_t + x} \right)^{1.62} \quad (10)$$

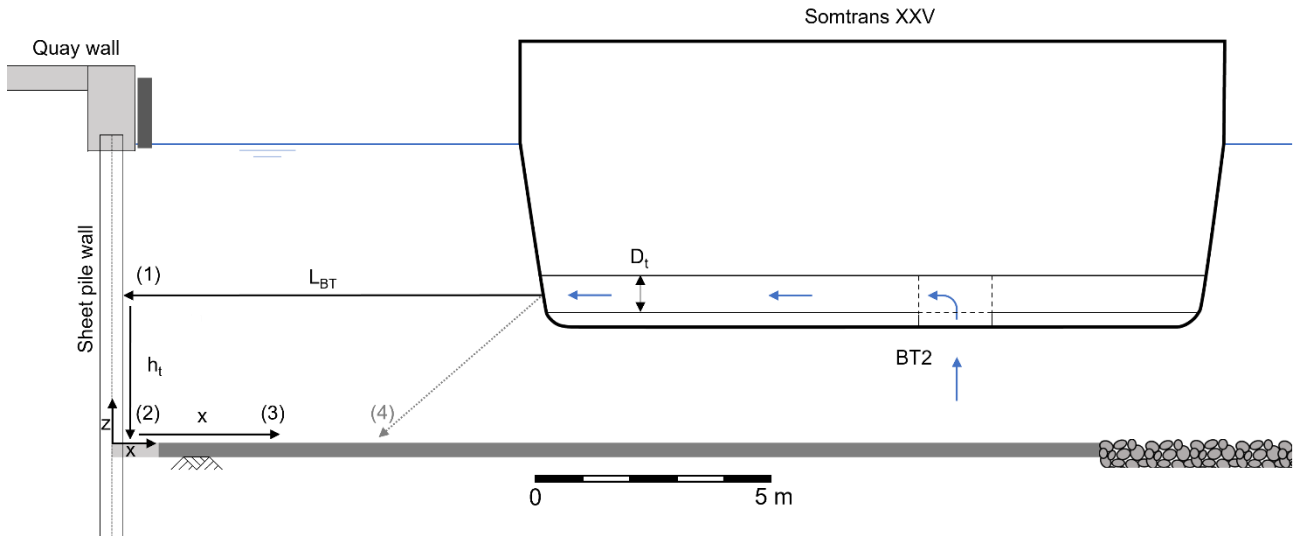


Figure 19: Cross-section of the quay wall and the vessel at BT2 including the location where the jet deflects on the quay wall (1), just after the intersection of the quay and the bed where the highest (virtual) flow velocities are expected (2), the decay in near-bed flow velocities in x-direction (3) and the location where the direct jet intersects with the bed (4) at $5.55 h_t$ from the bow thruster outlet (Blokland, 2018).

In Table 4 an overview is presented for the range in L_{BT} , h_t and locations of the measurement sensors in x -direction for the German method, Dutch method and Gent measurements. These parameters are made dimensionless by dividing them by the corresponding D_i of the research to compare the methods to the measurements in Gent. Please note that due to the measured deviation of Δx (recorded at BT2) from the predefined target value of Δx , an average deviation of 0.36 meters, calculated over Tests 1-21, has been accounted for. This adjustment is added to L_{BT1} and L_{BT2} for the considered tests in Figure 20 and Figure 21, ensuring a fair comparison with the guidelines.

Table 4: Range of the dimensionless quay wall clearance (L_{BT}/D_t), height of the bow thruster axis above the bed (h_t/D_t) and sensor locations (x/D_t) in x -direction for the German method, Dutch method and the Gent measurements.

Method	L_{BT}/D_t [-]	h_t/D_t [-]	Sensor locations x/D_t [-]
German (Schmidt, 1998)	3.97, 5.44, 7.28	1.66-3.93	0.29-3.38
Dutch (Blokland, 1996)	3.2, 6.2, 12	2.66-2.86 (tide)	0.49, 0.82, 1.47
Gent measurements	3.23 – 8.33	3.03	1.40, 2.94, 4.81, 6.81, 7.90

The results from the present Gent measurements for \bar{V}_{hor} and \bar{V}_x are compared to the theoretical predictions of the Dutch and German method respectively in Figure 20 for BT1 and Figure 21 for BT2. On the y-axis the near-bed flow velocity is presented as proportion of the theoretical efflux velocity V_0 for 25%, 50% and 90% power calculated according to Equation (5). On the x-axis the distance x from the quay wall divided by D_t is shown. In Figure 20a the upper limits per sensor location for $\Delta x = 0.8$ m or $L_{BT1}/D_t = 5.58$ (Test 3,9,11,12) are compared to the Dutch and German method. In Figure 20b the sensitivity of the methods to a larger quay wall clearance is investigated with $\Delta x = 3$ m or $L_{BT1}/D_t = 7.64$ (Test 20) for BT1. In a similar way in Figure 21a a comparison is made with the methods for the upper limits per sensor for $\Delta x = 0.8$ m or $L_{BT2}/D_t = 3.23$ (Tests 2,8,13,15) and for a larger quay wall clearance with $\Delta x = 3$ m or $L_{BT2}/D_t = 5.28$ (Test 19) in Figure 21b.

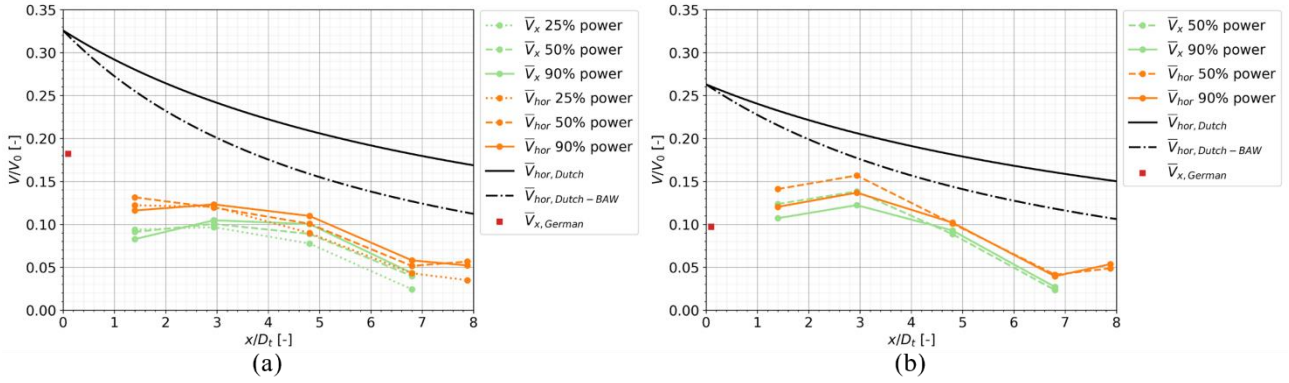


Figure 20: Comparison between the mean near-bed flow velocities as calculated with the Dutch and German method and measurements for BT1 in Gent. Where (a) is the upper limit per sensor for $\Delta x = 0.8$ m or $L_{BT1}/D_t = 5.58$ (Test 3,9,11,12) and (b) for a larger quay wall clearance of $L_{BT1}/D_t = 7.64$ ($\Delta x = 3$ m) during Test 20.

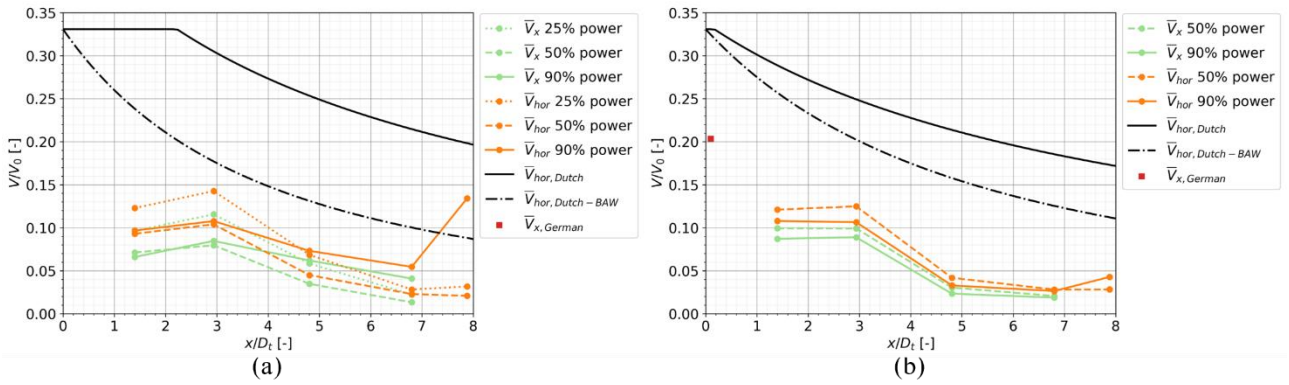


Figure 21: Comparison between the mean near-bed flow velocities as calculated with the Dutch and German method and measured for BT2 in Gent. Where (a) is the upper limit per sensor for $\Delta x = 0.8$ m or $L_{BT2}/D_t = 3.23$ (Test 2,8,13,15) and (b) the comparison for a larger quay wall clearance $\Delta x = 3$ m or $L_{BT2}/D_t = 5.28$ (Test 19). In (a) the German method results to the extreme value of $0.55 V/V_0$ falling outside the y-scale of $0.35 V/V_0$.

The comparison indicates that both the Dutch and German methods generally overestimate the measured near-bed flow velocities, thus being conservative. Two exceptions to this finding are observed. Firstly, Ott2 (fifth sensor) in Figure 21a shows a higher value for \bar{V}_{hor} than derived from $\bar{V}_{hor,Dutch-BAW}$. This discrepancy could not be explained with the current data. Secondly, the German method slightly underestimates \bar{V}_x for a quay wall clearance of $L_{BT1}/D_t = 7.64$ in Figure 20b. Figure 20 and Figure 21 demonstrate the high sensitivity of the German method to variations in quay wall clearances, overestimating \bar{V}_x for small quay wall clearances while slightly underestimating \bar{V}_x for larger quay wall clearances. The unusually high prediction of the German method of $0.55 V/V_0$ (see caption Figure 21) is most likely due to the quay wall clearance $L_{BT2}/D_t = 3.23$ falling outside the range of L_{BT}/D_t for which the German method is developed and validated (Table 4). Therefore, comparing measurement results to the Dutch and German method outside their applicability range should be done with caution.

Another observation is the fundamental difference in the guidelines and the measurement results for the influence of the quay wall clearance L_{BT} on the near-bed flow velocities. As the guidelines prescribe lower flow velocities for increasing quay wall clearances L_{BT} . For both BT1 and BT2 this relation is not observed. As for certain measurements slightly higher flow velocities are observed for a larger L_{BT} .

The dependency of the Dutch method on the total travelled distance by the jet to determine the decay profile of the near-bed flow velocity based on the sum of L_{BT} , h_t and x is not reflected by the measurement results. The decay in flow velocity is mostly influenced by the distance from the quay wall (x), irrespective of quay wall clearance L_{BT} . Therefore, the spreading of the jet in zone 2 as illustrated in Figure 1, characterized by decreasing flow velocities in the axis of the jet, is not reflected by the measurement results. Besides, the alternative Dutch method, $\bar{V}_{hor,Dutch-BAW}$ approaches the decay in measured near-bed flow velocities in Gent better than $\bar{V}_{hor,Dutch}$.

4.2 Relative turbulence intensity

The relative turbulence intensity (r) is defined as the root mean square of the turbulent fluctuations (V') divided by the mean flow velocity component (\bar{V}). According to current literature, the turbulence intensity near the bed should fall in the range of 0.25-0.30 based on measurements by Blaauw & van de Kaa (1978) and between 0.16-0.43, with an average of 0.3, according to Blokland (1996). Where Blaauw & van de Kaa (1978) measured r in the axis of the slipstream of an unrestricted propeller jet. While Blokland (1996) measured r near the bed for a deflected propeller jet on a vertical quay wall (Blokland, 1996). Furthermore, CIRIA et al. (2007) indicates values for r up to 0.6. However, these values are not based on actual turbulence measurements but on stone stability measurements (PIANC, 2015). For the measurement results r is calculated for the horizontal flow velocity component. In Figure 12b results for r_{hor} are illustrated falling in the range of 0.2-0.8, significantly larger than the values found in literature. An explanation can be found in the low mean flow velocities and high turbulent character of the reflected propeller jet. In addition, the large values for r_{hor} are mainly observed for ADV3 and ADV4 measuring the lowest mean flow velocities. Consequently, for the low mean flow velocities measured by these ADV3 and ADV4, the relative turbulence intensity may not be a reliable indicator of actual turbulence levels. This is because small fluctuations in velocity can result in disproportionately high relative turbulence intensity values, which may not accurately reflect the true turbulence characteristics of the flow. Focusing on ADV1 and ADV2, a range in r_{hor} of 0.3-0.6 is observed. Overall, average values over Test 1-21 for r_{hor} determined over ADV1-4 and the three different power steps are in the range of 0.4-0.47. Which is similar to the recommended value of $r = 0.45$ for stability calculations of the flow from a propeller jet (RWS/DHL, 1988).

4.3 Use of multiple bow thrusters

During the measurements in Gent several tests were conducted with both BT1 and BT2 activated simultaneously resulting in the highest hydraulic loads on the bed as illustrated in Figure 13. To consider multiple propellers two approaches are adopted in PIANC (2015). Either linear superposition or quadratic superposition. In linear superposition the velocities of the bow thrusters are simply added. In quadratic superposition the velocities of BT1 and BT2 are combined by $BT1\&2 = \sqrt{BT1^2 + BT2^2}$. For predicting the near-bed flow velocity for n equal bow thrusters using quadratic superposition results in multiplication of the velocity of one bow thruster by \sqrt{n} . It must be noted however that the maximum bed velocity induced by the jet using quadratic superposition is only valid for large distances behind the propeller/thruster. Which is not applicable to berthing operations with the vessel close to the quay wall. In Figure 22 the previously mentioned approaches are applied to the average near-bed flow velocity for the 90% power step from Figure 13 for V_{max} (Figure 22a) and \bar{V}_{hor} (Figure 22b). The best correspondence for V_{max} is linear superposition (BT1+BT2), although this overestimates the near-bed flow velocities for ADV1 and ADV2. For \bar{V}_{hor} linear superposition (BT1+BT2) results in very similar values as for BT1&2 activated simultaneously. Therefore, when only focusing on \bar{V}_{hor} while leaving σ_{hor} out of consideration linear superposition of BT1 and BT2 results in the expected near-bed flow velocity as induced by BT1&2.

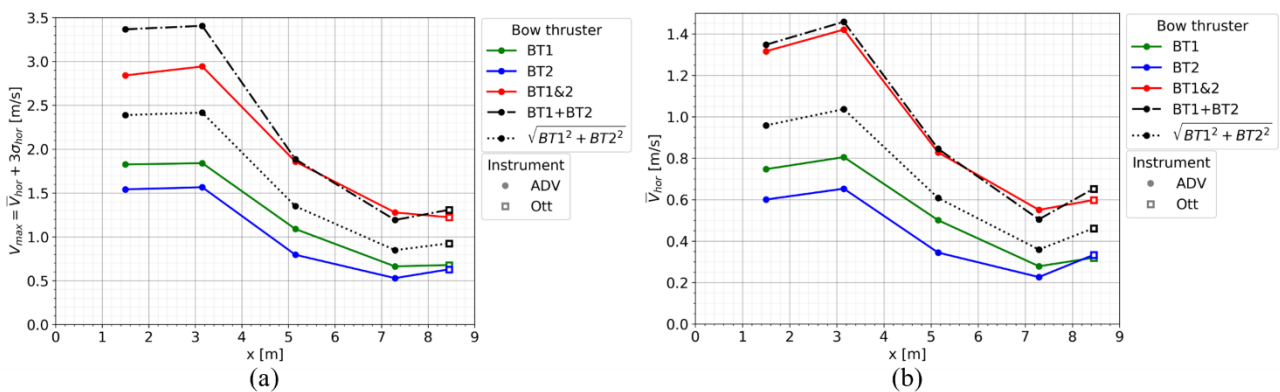


Figure 22: Comparison between linear superposition and quadratic superposition to determine the best fit for the near-bed flow velocity induced by BT1&2 based on the average results of the tests with BT1 (Test 3, 9, 11, 12 and 20) and BT2 (Test 2, 5, 8, 13, 15 and 19) for the 90% power step. (a) The comparison for V_{max} and (b) for \bar{V}_{hor} .

5 Discussion

5.1 Measurement set-up and protocol

Measurement set-ups and test programs for full scale measurements pose limitations compared to scale model tests. The first limitation of this study is the number of sensors measuring the flow velocity near the bed. Five sensors were positioned in line with each other in x-direction to determine the decay in near-bed flow velocities and an additional sixth sensor (Ott1) was placed besides ADV2 for data redundancy. To increase the number of measurements points, the vessel was moved in y-direction to create a matrix of measurement points, providing information on the location of the maximum flow velocity in both x- and y-direction. Physically, the blunt corner between the quay wall and the bed is expected to be a stagnation point with negligible quay-perpendicular velocities. Current guidelines (Dutch and German method) indicate that the maximum flow velocity occurs near the intersection of this corner. However, the results from Gent, shown in Figure 11a and Figure 12a, indicate that the highest near-bed flow velocity was measured at ADV2 at $x/Dt = 2.94$. A higher resolution in sensors near the quay could provide more insight on this matter and a more accurate location of the maximum flow velocity.

A second limitation is that during the field measurements, the influence of the sheet pile wall configuration on the reflected jet was not studied, leaving this influence unknown. Different configurations of sheet pile walls can affect the behavior of the reflected jet by altering flow patterns and turbulence characteristics. Variations in alignment, surface roughness, and structural features can cause the jet to deflect in various directions, affecting the distribution of flow velocities. For example, an angled wall may concentrate velocities in certain areas, while irregularities such as interlocking sections can create localized turbulence and swirling currents.

A third limitation is the number of measurements and duration of each measurement. Due to time restrictions choices were made in the number of measurements and the range in measurement parameters that could be researched. Only a few tests were repeated to research the redundancy in the measurement data. Nevertheless, by measuring for different power steps the results could be compared with each other by dividing the flow velocity by the corresponding theoretical efflux velocity (V_0) of that power step (Figure 20 and Figure 21) leading to similar decay profiles and values for V/V_0 .

A fourth limitation is the fixed height of the bow thruster axis above the bed resulting in one under keel clearance (UKC) of 2.52 m. Therefore, different under keel clearances (UKC) could not be realized during the full-scale measurements in Gent. Questions can be raised whether this UKC resulted in the highest hydraulic load on the bed.

The CEMT VIa Rijnmax class inland vessel was chosen for the measurements in Gent due to its large draught and minimal under keel clearances, simulating the highest hydraulic loads on the bed. The study focused on inland vessels, which typically feature a box-shaped hull with a flat bottom and vertical sides, unlike the V-shaped hulls of sea-going vessels. The limited space between the quay wall, hull, and bed can lead to higher flow velocities and greater impact on the bed, increasing frictional forces and resulting in more turbulent eddies and vortices. However, the rectangular channel shape and the propeller's position at the bow thruster entrance minimize the jet's swirling motion.

Another limitation observed was the precision in positioning the vessel in x- and y-direction. Due to the tension in the lines and the inherent constraints in accurately positioning the vessel, deviations from the target values of Δx and Δy were noted, as detailed in Table 3. Deviations from the target value Δx had an average of 0.36 m with a standard deviation of 0.30 m, while for Δy the deviations were significantly smaller with an average deviation and standard deviation of both 0.08 m. Therefore, only the deviations of Δx are encountered for in section 4 and listed in Table 3.

To ensure repeatability and consistency, the tests were conducted at a location with negligible flow and no other vessels present, within a short two-day period under constant environmental conditions. Two pairs of tests (Test 5 and 8 during 25% and 90% power, and Test 10 and 17 during 50% power) were repeated under nearly identical conditions. The average relative difference in maximum velocity ($\bar{V}_{hor} + 3\sigma_{hor}$) for these pairs of tests was found to be 21.4%.

5.2 Comparison of the measurement results to literature

The measurement results were compared to the Dutch and German method for determining the near-bed flow velocities induced by a reflected bow thruster jet on a vertical quay wall as prescribed by the PIANC (2015) guidelines. The measurement results are compared to the guidelines by dividing the measured near-bed flow velocity over the theoretical efflux velocity V_0 resulting in the relative flow velocity (V/V_0). However, as the actual efflux velocity V_0 is not measured, V_0 is determined by Equation (5) which is not based on efflux velocity measurements for channel type bow thrusters. This poses the largest uncertainty for the comparison to the guidelines and might be an explanation for the limited change in measured flow velocity between 50% and 90% power. Furthermore, whether V_0 is defined as the cross-sectional averaged efflux velocity or the maximum efflux velocity from the bow thruster channel is unclear. Therefore, using V_0 leads to uncertainty in the comparison between the measurement results and the Dutch and German method. In addition, the Dutch method is based on field measurements with a tugboat while the German method is founded upon scale model measurements where the vessel and bow thruster are based on a sea-going vessel. Thus, comparing these methods to the measurements in Gent with an inland vessel having a different hull shape and bow thruster system (channel system) poses limitations and uncertainties that must be noted in any conclusions drawn on this comparison.

Schmidt (1998) identified five different zones in the simplified 2D x - z cross-section for the bow thruster jet reflecting on a vertical quay wall as illustrated in Figure 1. Although the measurements only focused on the near-bed flow velocity, a comparison to the five zones identified by Schmidt (1998) can be made. The first zone is the region of flow establishment of the jet where the velocity in the axis of the jet equals the efflux velocity. The length of this zone is 2.6 (Fuehrer, Pohl, & Römis, 1987) or 2.8 D_t (Blaauw & Van de Kaa, 1978). In the second zone the flow is established, the jet spreads and decreases in flow velocity. The vessel was moored to the quay ($\Delta x = 0.8$ m) with an average $L_{BT1} = 5.58 D_t$ and $L_{BT2} = 3.23 D_t$. Therefore, according to literature both jets are in the zone of established flow before the jet deflects on the quay wall. Although being in the zone of established flow, for very small quay wall clearances of BT2 increasing L_{BT} does not lead to lower but higher near-bed flow velocities (Figure 17a) according to the measurement results. Deltares (2015) found that for very small quay wall clearances in the order of 1.5 D_t the quay wall hindered the outflow of the propeller jet resulting in lower flow velocities near the bed. Thus, for very small quay wall clearances, which are not adopted in theoretical methods such as the German and Dutch method, lower near bed flow velocities can be expected.

From Section 4 it is observed that the Dutch and German method lead to conservative near-bed flow velocities with respect to the measurement results. Especially for small quay wall clearances the German method significantly overestimates the near-bed flow velocity with respect to the measurement results. For larger quay wall clearances, the German method gives a good estimation. Compared to previous scale model measurements by Deltares (2015) with relatively small quay wall clearances of 1.5 and 5.5 D_t , the Dutch method was also conservative. However, underestimating the near-bed flow velocity for a large quay wall clearance of 9.5 D_t . Furthermore, Deltares (2015) concluded that the alternative Dutch method according to Equation (10) underestimates the near-bed flow velocities. This contradicts the results presented in Figure 20 and Figure 21 for the Gent measurements. In addition, Deltares (2015) found that the maximum near-bed flow velocity did not always occur near the quay wall. During field measurements with an inland vessel Cantoni (2020) observed smaller flow velocities than expected based on current guidelines during measurements with small quay wall clearances ($\leq 4.23 D_t$). Possible explanations were the rectangular shape of the hull of the inland vessel, leading to a more confined flow in comparison to the measurements with a v-shaped hull of a seagoing vessel (German method) or a tugboat (Dutch method). Furthermore, the used channel bow thruster system could also lead to smaller near-bed flow velocities in comparison to current guidelines. The previously mentioned studies and the results from the measurements in this study emphasize that the current design guidelines do not result in accurate predictions of near-bed flow velocities. Especially for inland vessels with a small quay wall clearance. During berthing of inland vessels, a small quay wall clearance is very common for bow thrusters due to the rectangular shape of the hull (Figure 3).

Although the flow pattern around the bow thruster axis is not extensively researched during the measurements in Gent, a pattern for the location of the maximum near-bed flow velocities is observed from Figure 14-Figure 16 in the direction of the stern of the vessel. These findings are confirmed by Deltares (2015) showing a general asymmetric flow pattern near the bed along the quay wall in the direction of the stern of the vessel. Nevertheless, other models such as the computational fluid dynamics model by van Blaaderen (2005) suggests a more symmetric pattern around the bow thruster

axis after reflection of the jet on the bed. Therefore, further research is advised as the flow pattern could influence the location of the maximum flow velocity which is of importance to consider in bed protection designs (Deltares, 2015).

The PIANC (2015) guidelines consider two methods for combining multiple bow thrusters: linear and quadratic superposition. Quadratic superposition applies only for large distances behind the thruster and is not suitable for berthing operations. Therefore, in Gent, only linear superposition (BT1+BT2) is relevant and closely matched the measured \bar{V}_{hor} , but overestimated for V_{max} at ADV1 and ADV2. Furthermore, this method does not account for factors like bow thruster type, channel length, bow thruster outlet shape, bow thruster propeller location and shape of the vessel.

The evaluation of bed protection design at the Moervaart quay wall in the North Sea Port Gent reveals that, when the measured near-bed flow velocities are used as the sole input to calculate the required bed protection, significantly smaller rock sizes and asphalt mattress thickness would be necessary to withstand the hydraulic load of the jet in comparison to current guidelines (PIANC, 2015). Further research is needed to determine whether this finding is generally applicable.

6 Conclusions

Field measurements are presented of near-bed velocities induced by a large (CEMT VIa Rijnmax) inland vessel with two 394 kW 4-channel bow thrusters. Several conclusions are drawn about the overall decay profile of near bed velocities. This includes the influence of the global measurement parameters; thruster power, quay-wall clearance, and along-quay displacement. Moreover, comparisons are made with theoretical guidelines for the hydraulic load and bed protection design. Lastly the performance of the measurement set-up is evaluated.

A general decay pattern was observed for almost every test with the highest near-bed flow velocities measured close to the quay wall within the first 4 m (ADV1 and ADV2) after which velocities rapidly decline towards a more constant level around 7 m from the quay wall. Opposed to current literature, the highest flow velocities near the bed are not measured at the first sensor ADV1 but at ADV2 at approximately 3 m from the quay wall. Close to the quay wall values for \bar{V}_{hor} range between 0.6-1.6 m/s with an average of 1 m/s decreasing towards values ranging between 0.1-1.0 m/s with an average of 0.4 m/s further from the quay near the bow thruster inlet. The defined maximum flow velocity ($V_{max} = \bar{V}_{hor} + 3\sigma_{hor}$) ranges between 1.6-3.4 times \bar{V}_{hor} . The decay in σ_{hor} shows a similar trend as \bar{V}_{hor} leading to relative turbulence intensities in the order of 0.3-0.6 at ADV1 and ADV2 close to the quay wall. Which is slightly higher than the range of 0.25-0.43 listed in literature.

Looking at the main measurement parameters altered during the measurements, increasing the applied power from 25% to 50% results in significantly higher flow velocities near the bed. However, further increasing towards 90% power leads to similar although slightly higher flow velocities in comparison to 50% power. Focusing on the used bow thruster, using BT1 resulted in the highest flow velocities near the bed. When BT1&2 are used simultaneously the mean near-bed flow velocities are best approached by linear superposition of the measured mean velocities of BT1 and BT2. Increasing the quay wall clearance of the bow thruster (L_{BT}) by moving the vessel further from the quay wall results in similar but slightly lower flow velocities. The exception to this trend is BT2 having a small quay wall clearance. As increasing L_{BT2} from 3.09 m to 5.29 m results in higher flow velocities. This could be explained by the fact that the jet of BT1 has more space to develop. Therefore, there is an optimum quay wall clearance at which the highest flow velocities are measured. Beyond this point, increasing L_{BT} results in decreased flow velocities. The highest flow velocities were not always measured directly beneath the bow thruster axis. Generally, near the quay wall, the highest flow velocities occur directly beneath the bow thruster axis. However, at greater distances x from the quay wall, the highest flow velocities are measured towards the stern of the vessel.

The theoretical upper limit for the mean near-bed flow velocities, calculated with the Dutch (\bar{V}_{hor}) and German (\bar{V}_x) method, significantly overestimate the upper limit for the measured near-bed flow velocities in Gent for almost every test. In addition, the decay in flow velocities for increasing distance x from the quay wall described by the Dutch method is not strong enough compared to the measurements. The adapted Dutch-BAW approach has a better resembling, though still overestimating in comparison to the measurements.

The current measurement set-up and program resulted in useful results on the decay in bow thruster induced near-bed flow velocities in x - and y -direction. Measuring with ADVs and Ott meters led to confidence in the sensors. From the measurements with the ADVs can be concluded that most energy of the jet is within the first 10 Hz of the frequency

spectrum. Therefore, measuring as high as 64 Hz is unnecessary to capture the turbulent fluctuations of the jet near the bed. A lower sampling frequency of 16 or 32 Hz leads to reduced noise within the signal. Comparing the manoeuvring measurement to the moored measurements leads to a similar decay profile in x -direction. Measuring lower velocities during the manoeuvring measurements than during the moored measurements.

Acknowledgements

The authors would like to thank all companies involved in the CROW Propeller Jet workgroup for their input, support, and hospitality. In particular, the North Sea Port Gent, Somtrans, Boskalis, and the Port of Rotterdam for their support and for providing the fully loaded Somtrans XXV for the field measurements.

Funding

The support by Rijkswaterstaat, Delft University of Technology, Port of Rotterdam, North Sea Port Gent, Boskalis and Somtrans is acknowledged.

Author contributions (CRediT)

Tukker, J.W.T.: Conceptualization, Data curation, Formal Analysis, Investigation, Methodology, Software, Validation, Visualization, Writing – original draft;

Ruijter, M.: Supervision, Data curation, Resources, review;

Van der Vorm-Hoek, C.V.A.: Resources, Project administration, Funding acquisition, Supervision, review;

Hofland, B.: Methodology, Supervision, Writing – review & editing.

Data access statement

The data acquired in the study will be made available on request.

Declaration of interests

The author(s) report(s) no conflict of interest.

Notations

Name	Symbol	Unit
Coefficient for the German method to determine \bar{V}_x	a_L	-
Circular bow thruster diameter	D_t	m
Water depth	h	m
Height of the bow thruster axis above the bed	h_t	m
Quay wall clearance of the considered bow thruster	L_{BT}	m
Installed bow thruster power	P_t	kW
Relative turbulence intensity (σ/\bar{V})	r	-
Flow velocity	V	m/s
Turbulent fluctuations of the flow velocity	V'	m/s
Flow velocity in x -direction	V_x	m/s
Flow velocity in y -direction	V_y	m/s
Flow velocity in horizontal direction composed out of the x and y component	V_{hor}	m/s
Average flow velocity	\bar{V}	m/s
Average flow velocity in x -direction	\bar{V}_x	m/s
Average flow velocity in horizontal direction composed out of the x and y component	\bar{V}_{hor}	m/s
Average flow velocity in x -direction determined with to the German method	$\bar{V}_{x,German}$	m/s
Average flow velocity in x -direction determined with the Dutch method	$\bar{V}_{hor,Dutch}$	m/s
Average flow velocity in horizontal direction determined with the alternative Dutch method from the BAW	$\bar{V}_{hor,Dutch-BAW}$	m/s
Efflux velocity of the bow thruster jet	V_0	m/s
Maximum flow velocity defined as the mean flow velocity plus three times the standard deviation ($\bar{V} + 3\sigma$)	V_{max}	m/s
Maximum instantaneous flow velocity	$V_{max,inst}$	m/s
Standard deviation to the mean flow velocity	σ	m/s
Reduction factor for the efflux velocity dependent on bow thruster type	ξ	-
Density of the water	ρ_w	kg/m ³
Distance in x -direction between the port side of the vessel and the sheet pile wall	Δx	m
Distance in y -direction between the considered bow thruster axis and sensors	Δy	m
Acoustic Doppler Velocimeter	ADV	-
Ott C31 current meter	Ott	-

References

- Abramowicz-Gerigk, T., Burciu, Z., Górski, W., & Reichel, M. (2018). *Full scale measurements of pressure field induced on the quay wall by bow thrusters – indirect method for seabed velocities monitoring*. Ocean Engineering volume 162, 2018, Pages 150-160, ISSN 0029-8018, <https://doi.org/10.1016/j.oceaneng.2018.05.036>.
- Albertson, M. L., Dai, Y. B., Jensen, R. A., & Rouse, H. R. (1950). Diffusion of submerged jets. *Transcript of the A.S.C.E., Paper No.2409, 115, 639-697*.
- BAW. (2010). BAW Code of Practice: Principles for the Design of Bank and Bottom Protection for Inland Waterways (GBB). *Federal Waterways Engineering and Research Institute, Karlsruhe*.
- Berger, W., Felkel, K., Hager, M., Oebius, H., & Schale, E. (1981). *Courant provoqué par les bateaux protection des berges et solution pour éviter l'érosion du lit du Haut Rhin*. Proceedings of the 25th Congress on P.I.A.N.C., Edinburgh, 1981, Section I-1.
- Blaauw, H. G., & Van de Kaa, E. J. (1978). Erosion of Bottom and Sloping Banks Caused by the Screw Race of Manoeuvring Ships. *Publ.no.202, Reprint of paper presented at the 7th International Harbour Congress, May 22-26, 1978, Antwerp., Delft Hydraulics Laboratory, The Netherlands*.

- Blokland, T. (1996). Bodembeschermingen belast door schroefstralen. Huidige ontwerpmethodiek. *Gemeentewerken Rotterdam, Ingenieursbureau havenwerken, Rapport 61.00-R94.038*.
- Blokland, T. (2018). 'Standaardisatie Maritieme Infrastructuur Havenbedrijf Rotterdam'. Rotterdam: Port of Rotterdam.
- Cantoni, I. (2020). *Bowthruster-induced flow on the bottom of a vertical quay wall*. Master's thesis, TU Delft.
- Cantoni, I., Van Der Hout, A., Houwing, E., Roubos, A., & Ruijter, M. (2023). Field Measurements of Flow Velocities in Propeller Jets. In: Li, Y., Hu, Y., Rigo, P., Lefler, F.E., Zhao, G. (eds) *Proceedings of PIANC Smart Rivers 2022. PIANC 2022. Lecture Notes in Civil Engineering*, vol 264. Springer, Singapore. https://doi.org/10.1007/978-981-19-6138-0_8.
- CIRIA, CUR, CETMEF. (2007). "The Rock Manual. The use of rock in hydraulic engineering" (2nd edition). *Manual on the Use of Rock*.
- Deltares. (2015). *Propeller jets, Knowledge gap 7 - Reflection of transverse jets by vertical quay walls, Report number 1210140-000-HYE-0008*.
- Deltares. (2018). *Veldmetingen schroefstraalbelastingen (memo in Dutch), project number 11202175*.
- DHI. (2016). *Computational Fluid Dynamics (CFD) modeling of propeller-induced flows on an inclined slope*. Hamburg Port Authority AöR, Project number 14802928.
- Durgesh, V., Thomson, J., Richmond, M. C., & Polagye, B. (2014). Noise correction of turbulent spectra obtained from acoustic doppler velocimeters. *Flow Measurement and Instrumentation Volume 37*, 29–41, ISSN 0955-5986.
- Fuehrer, M., & Römis, K. (1977). Effects of modern ship traffic on inland and ocean waterways and their structures. *PIANC 24th congress, section 1-3*.
- Fuehrer, M., Pohl, H., & Römis, K. (1987). Propeller jet erosion and stability criteria for bottom protection of various constructions. *Proceedings of P.I.A.N.C., Bulletin No. 58, 1987*.
- Fuehrer, M., Römis, K., & Engelke, G. (1981). Criteria for dimensioning the bottom and slope protections and for applying the new methods of protecting navigation canals. *PIANC XXVth Congress*.
- Goring, D., & Nikora, V. (2002, January). Despiking Acoustic Doppler Velocimeter Data. *Journal of Hydraulic Engineering-asce - J HYDRAUL ENG-ASCE*, 128. doi:10.1061/(ASCE)0733-9429(2002)128:1(117)
- Hamill, G., & Kee, C. (2016). Predicting axial velocity profiles within a diffusing marine propeller jet. *Ocean Engineering* 124, 104–112.
- Hoffmans, G., & Verheij, H. (2011). *Jet scour*. Proceedings of the Institution of Civil Engineers - Maritime Engineering, 164(4), 185-193.
- Huang, C., Qiao, F., & Ma, H. (2020, January). *Noise reduction of acoustic Doppler velocimeter data based on Kalman filtering and autoregressive moving average models*. doi:<https://doi-org.tudelft.idm.oclc.org/10.1007/s13131-020-1641-x>
- Izbash, S. (1935). *Construction of Dams by Dumping Stones into Flowing Water. (Постройка плотин наброской камня в текущую воду)*. Scientific Research Institute of Hydrotechnics, USSR.
- Johnston, H., Hamill, G., Wilson, P., & Ryan, D. (2013). *Influence of a boundary on the development of a propeller wash*. Ocean Engineering, Volume 61, Pages 50-55, ISSN 0029-8018, <https://doi.org/10.1016/j.oceaneng.2012.12.033>.

- Lam, W., Hamill, G. A., Song, Y. C., Robinson, D. J., & Raghunathan, S. (2011). *A review of the equations used to predict the velocity distribution within a ship's propeller jet*. Ocean Engineering.
- Looye, N. (2021). *Schaalvergroting binnenvaart (Dutch)*. Utrecht: Rijkswaterstaat.
- Meijer, D. G., & Verheij, H. J. (1993). *"Stroomsnelheden bij de oever veroorzaakt door boegschroeven"*. Waterloopkundig Laboratorium.
- Nortek. (2018). *The comprehensive manual for velocimeters*. Nortek AS.
- Nortek. (2024). *Vector - 300 m technical specifications*. Retrieved from Nortekgroup.com: <https://www.nortekgroup.com/products/vector-300-m/pdf>
- OECD, I. (2015). The impact of mega-ships. https://www.itf-oecd.org/sites/default/files/docs/15cspa_mega-ships.pdf. International Transport Forum.
- OTT-HydroMet. (2021). *OTT C31*. Retrieved from <https://www.ott.com/products/water-flow-3/ott-c31-958/>
- PIANC. (2015). Guidelines for Protecting Berthing Structures From Scour Caused by Ships. *Report No. 180*.
- Pilarczyk, K. W. (1996). *Offshore breakwaters and shore evolution control*. Rotterdam: Balkema.
- Raes, L., Elskens, F., Römisch, k., & Sas, M. (1996). "The effects of ship propellers on bottom velocities and on scour near berths and protection methods using thin flexible revetments". Proc. 11th Intern. Harbour Congress, Antwerp.
- Rijkswaterstaat. (2020). *Richtlijn Ontwerp Waterbouw, ROW Versie 2 (Dutch)*.
- Roubos, A., & Verhagen, H. J. (2007). Uncertainties in the design of bed protections near quay walls. *4th International Conference Port Development and Coastal Environment: PDCE 2007, 25-27 September 2007, Varna, Bulgaria*.
- Roubos, A., Blokland, T., & van der Plas, T. (2014). *Field tests propeller scour along quay wall*. PIANC World Congress San Francisco.
- RWS/DHL. (1988). *Aantasting van Dwarsprofielen in Vaarwegen (in Dutch)*. Report M1115 XIX.
- Schiereck, G., & Verhagen, H. (2016). *Introduction to bed, bank and shore protection*. Delft: Delft Academic Press.
- Schmidt, E. (1998). *Ausbreitungsverhalten und Erosion swirkung eines Bugpropellerstrahls vor einer Kaiwand*. Dissertation am Leichtweiss-Institut für Wasserbau der Technischen Universität Braunschweig.
- Tukker, J. (2021). *Decay of bow thruster induced near-bed flow velocities*. TU Delft.
- van Blaaderen, E. (2005). *Modelling bowthruster induced flow near a quay wall*. Master thesis, TU Delft.
- Verheij, H. J. (1983). The stability of bottom and banks subjected to the velocities in the propeller jet behind ships. *8th Int. Harbour Congress, Antwerp*.
- Weenen, R. d., Geest, W. v., Hindriks, I., & Grijspaardt, T. (2020). *Middenlange termijn prognoses voor de binnenvaart (Dutch)*, <https://archieff.panteia.nl/default/assets/File/Middellange%20termijn%20prognoses%20voor%20het%20ladingvolume%20in%20de%20binnenvaart%202020%20-%202025%2022112020.pdf>. Zoetermeer: Panteia.
- Wei, M., & Chiew, Y. (2019). Impingement of propeller jet on a vertical quay wall. *Ocean Engineering* 183, 73-86.

- Wei, M., Chiew, Y. M., & Hsieh, S. C. (2017, October). Plane boundary effects on characteristics of propeller jets. *Experiments in Fluids*, 58, 141. doi:10.1007/s00348-017-2425-8
- Welch, P. (1967). The use of the fast Fourier transform for the estimation of power spectra: A method based on time averaging over short, modified periodograms. *IEEE Trans. Audio Electroacoust.* vol. 15, pp. 70-73.

Annex A

In this annex, the metadata for the moored (Test 1-21) and manoeuvring tests (Test 22-24) is provided. Below is an explanation of the various parameters listed in the columns of Table 5.

- **Test:** number of the measurement tests, ranging from 1-24. Test 6 and 7 are excluded as they were load cell tests not further analyzed within this study.
- **Vessel position:** A total of six different vessel positions were used, as illustrated in Figure 6, Figure 7 and Figure 8.
- **Bow thruster:** The bow thruster used during the tests.
- **Power percentage [%]:** The power percentage read from the bridge of the vessel during the measurements.
- **RPM:** The RPM read from the bridge of the vessel during the measurements.
- **DateTime and Duration:** The start time and duration of each test.
- y_{port} : The y-coordinate measured during the tests using a measurement line attached to the vessel. The distance between y_{port} and y_{BT2} was 21 m.
- y_{BT2} : Derived from y_{port} to determine the y-coordinate at the location of the axis of BT2.
- x_{port} : Measured with a laser distance measurement device for each test.
- x_{BT2} : Measured with a laser distance measurement device for each test.

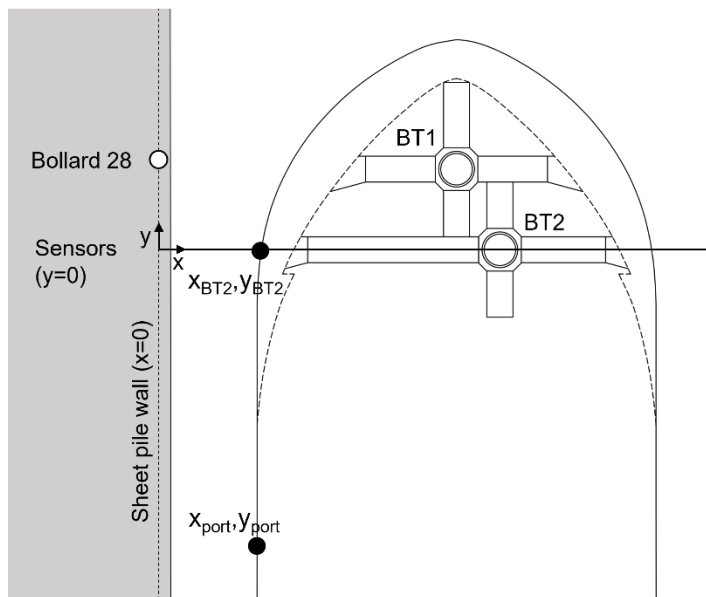


Figure 23: Top view of the outlines of the vessel at the quay wall with the locations of y_{port} , x_{port} , y_{BT2} and x_{BT2} of which the metadata was administered during the measurements as listed in Table 5.

Table 5: Metadata of the field measurements in Gent.

Test	Vessel position	Bow thruster	Power percentage [%]	RPM	Datetime [dd/mm/yyyy hh:mm:ss]	Duration [hh:mm:ss]	y _{port}	x _{port}	y _{BT2}	x _{BT2}
1	1	2	28-29%	1064	30/09/2020 11:47:37	00:02:33	-20.95	1.45	0.05	1.85
			49%	1412-1420	30/09/2020 11:50:54	00:08:25	-20.95	1.45	0.05	1.85
2	1	2	30%	1063	30/09/2020 13:00:34	00:01:30	-21.05	1.31	-0.05	1.69
			50%		30/09/2020 13:03:16	00:07:44	-21.05	1.31	-0.05	1.69
			90%		30/09/2020 13:13:16	00:02:54	-21.03	1.46	-0.03	1.82
3	1	1	25%	920	30/09/2020 14:48:18	00:02:42	-21.00	0.96	0.00	1.24
			50%	1461-1463	30/09/2020 14:51:49	00:01:54	-21.00	0.96	0.00	1.24
			85%	1800	30/09/2020 14:53:55	00:02:26	-21.00	0.96	0.00	1.24
4	1	1 & 2	25%	938-944	30/09/2020 14:57:05	00:03:15	-21.00	1.01	0.00	1.45
			50%	1460-1470	30/09/2020 15:00:56	00:02:42	-21.00	1.21	0.00	1.68
			85%	1800	30/09/2020 15:04:10	00:03:22	-21.00	1.28	0.00	1.77
5	2	2	25%	970	30/09/2020 15:15:08	00:02:52	-23.00	0.88	-2.00	1.22
			88%	1813	30/09/2020 15:21:13	00:03:22	-23.00	1.58	-2.00	1.97
8	2	2	27%	1063	30/09/2020 16:00:12	00:02:48	-22.92	1.43	-1.92	1.92
			87%	1810	30/09/2020 16:03:11	00:02:19	-22.92	1.47	-1.92	1.94
9	2	1	25%	940	30/09/2020 16:05:55	00:02:13	-22.92	1.44	-1.92	1.91
			50%	1470	30/09/2020 16:08:11	00:02:30	-22.92	1.44	-1.92	1.91
			85%	1800	30/09/2020 16:11:08	00:02:22	-22.92	1.46	-1.92	1.97
10	2	1 & 2	25%	950	30/09/2020 16:19:48	00:02:38	-23.00	1.45	-2.00	1.98
			50%	1480	30/09/2020 16:23:10	00:01:50	-23.00	1.49	-2.00	2.00
11	5	1	25%	940	01/10/2020 09:22:08	00:02:46	-26.44	0.80	-5.44	1.19
			50%	1485	01/10/2020 09:25:43	00:02:27	-26.44	0.82	-5.44	1.19
			84%	1800	01/10/2020 09:28:39	00:02:58	-26.39	0.95	-5.39	1.31
12	4	1	25%	937	01/10/2020 09:36:04	00:03:31	-24.39	0.80	-3.39	1.16
			50%	1443	01/10/2020 09:40:05	00:01:53	-24.39	0.80	-3.39	1.17
			90%	1803	01/10/2020 09:42:07	00:02:37	-24.37	0.84	-3.37	1.24
13	4	2	29%	1063	01/10/2020 09:46:35	00:02:08	-24.39	0.80	-3.39	1.15
			89%	1810	01/10/2020 09:48:51	00:02:06	-24.37	0.84	-3.37	1.23
14	4	1 & 2	25%	945-950	01/10/2020 09:51:26	00:02:36	-24.37	0.81	-3.37	1.19
			50%	1470-1473	01/10/2020 09:54:36	00:02:09	-24.32	0.97	-3.32	1.4
			86%	1798-1800	01/10/2020 09:57:06	00:02:06	-24.24	0.97	-3.24	1.62

15	3	2								
			86%	1810	01/10/2020 10:08:10	00:02:20	-18.74	0.80	2.26	1.15
16	3	1 & 2								
			25-26%	952-954	01/10/2020 10:11:08	00:02:20	-18.74	0.80	2.26	1.16
			50%	1475-1480	01/10/2020 10:13:43	00:02:28	-18.74	0.80	2.26	1.21
			85-86%	1800-1804	01/10/2020 10:16:26	00:02:25	-18.63	0.94	2.37	1.35
17	6	1 & 2								
			50-55%	1480-1485	01/10/2020 10:41:52	00:04:06	-22.78	1.19	-1.78	1.64
			87%	1800	01/10/2020 10:46:09	00:02:33	-22.78	1.27	-1.78	1.74
18	7	1 & 2								
			50%	1480	01/10/2020 10:52:50	00:01:56	-22.72	2.97	-1.72	3.8
			85%	1800	01/10/2020 10:55:46	00:02:14	-22.71	3.08	-1.71	3.94
19	7	2								
			50%	1432	01/10/2020 10:58:49	00:02:29	-22.71	3.01	-1.71	3.85
			95%	1810	01/10/2020 11:01:27	00:02:23	-22.71	3.04	-1.71	3.88
20	7	1								
			50%	1470	01/10/2020 11:04:27	00:02:03	-22.71	3.01	-1.71	3.87
			89%	1800	01/10/2020 11:06:40	00:02:46	-22.71	3.03	-1.71	3.88
21	8	1 & 2								
			49-50%	1463-1465	01/10/2020 11:14:43	00:02:22	-22.70	4.77	-1.7	5.94
			85%	1800	01/10/2020 11:17:30	00:03:02	-22.70	4.90	-1.7	6.12
22	Berthing	1 & 2								
			25%	932	01/10/2020 11:37:58	00:01:32	Initial 22.75	Initial -1.75	0.8 to 15 m	
			25%	932	01/10/2020 11:39:30	00:02:56	Initial 22.75	Initial -1.75		
			48%	1440-1445	01/10/2020 11:42:38	00:01:22	Initial 22.75	Initial -1.75	0.8 to 15.9 m	
			48%	1440-1445	01/10/2020 11:44:00	00:01:33	Initial 22.75	Initial -1.75		
			87%	1800	01/10/2020 11:48:42	00:00:48	Initial 22.75	Initial -1.75	0.8 to 11.3 m	
			87%	1800	01/10/2020 11:49:31	00:02:26	Initial 22.75	Initial -1.75		
23	Sailing	1 & 2								
			80%	1700	01/10/2020 11:59:40	00:02:41		4.25	-10 to +10	
24	Sailing	1								
			97%	1805	01/10/2020 12:08:07	00:02:59		4.25	-10 to +10	